

Response to Reviewer #1

We thank the Reviewer for his/her appreciation of our work and appreciate his/her helpful comments. Below, we reply to his specific comments (reported in italics)

Minor Comments.

Pg. 4430, Ln. 20: It would be useful to have a little more information in the manuscript about how TT2010 explained the dynamics of the impact of the Dalton Minimum on the PNA. It is mentioned that the solar minimum was implicated in the event, but a slightly more complete discussion of the full dynamical chain from the TOA forcing to the PNA response would be useful.

TT2010 did not discuss the full dynamical chain from the TOA forcing to the PNA response, which is also beyond the scope of this study. In the revised version of the manuscript, we have shortly extended the part on the TSI-PNA link, based on the discussion in TT2010.

Pg. 4433, Ln. 17: Three regions are vague here. Please refer to a figure or be more specific about the regions considered. This is clarified later in this text, but it would be useful to have it at this point.

Will do

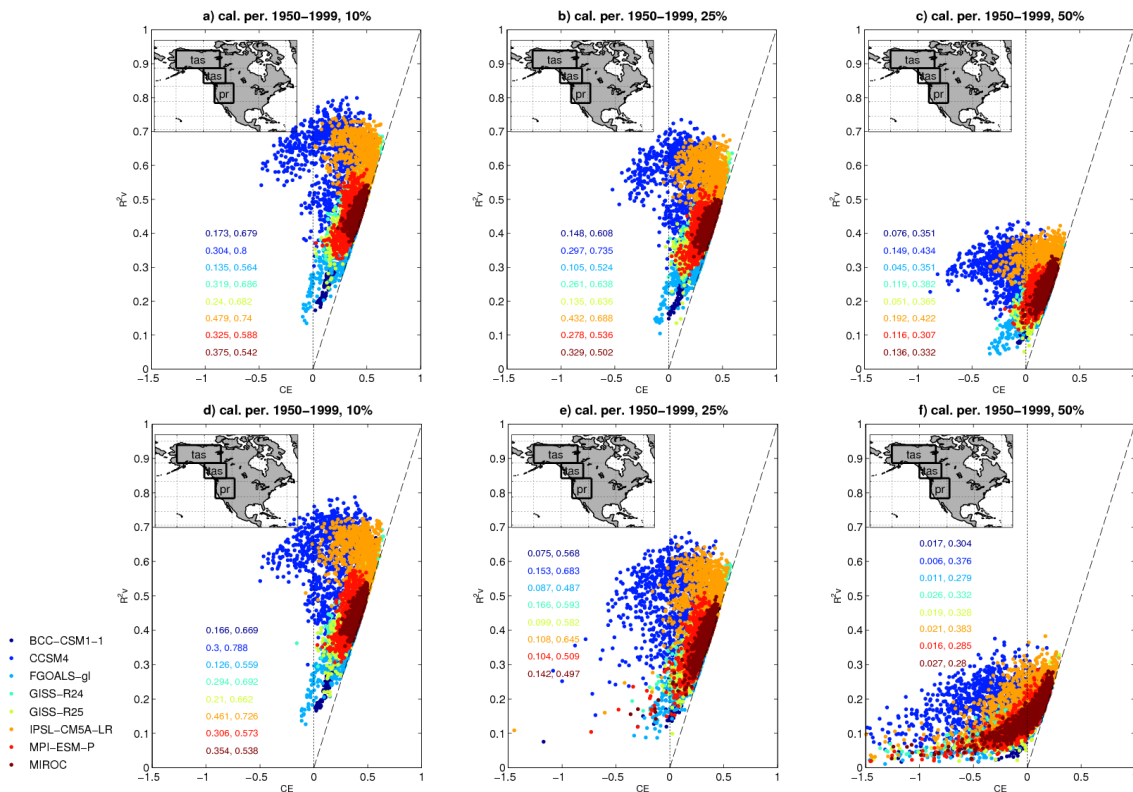
Pg. 4433, Ln. 24: My biggest concern with the manuscript comes at this point. The authors do not reasonably justify why they use perfect pseudoproxies. It is standard practice to perturb the pseudoproxies with noise to mimic the imperfect connection between climate and proxies in the real world. This has been shown to be important in numerous studies regarding the impact on reconstruction skill. This is reviewed in Smerdon (WIREs Clim. Ch., 2012) and recent studies that have attempted to more realistically emulate the character of noise in real-world proxies have shown important additional impacts. For instance, Wang et al. (Climate of the Past, 2014) and Evans et al. (GRL, 2014) have both addressed the realism of various reconstruction problems and shown that more realistic additions to the pseudoproxy construction yield reduced skill. The latter study is particularly relevant to the present work, given that the authors model tree-ring chronologies and show that more realistic tree-ring predictors reduce the skill of their pseudoproxy reconstructions. The authors should further justify their use of perfect pseudoproxies or include an experiment with the addition of noise to the pseudoproxy predictors.

As we stated on page 4434, lines 21-24 of the discussion paper, “we aim at testing PNA reconstructions based solely on local geophysical predictors from northwestern North America, not at replicating the linkage between biological sensors and the local environmental forcing at the basis of the TT2010 reconstruction”. So, our goal is to compare pseudo-reconstructions and targets under the idealized hypothesis that the considered proxies provide perfect information about the local climate conditions. This is why, on discussing our results we focused only on those predictors yielding the highest skills among the considered random sets: we wanted to delineate the upper bound of this reconstruction method, revealing the “inherent limitations of a PNA reconstruction method solely relying on local geophysical predictors from northwestern North America” (page 4444, lines 16-18). Including realistic noise levels in proxies would complicate this already complex/thorough investigation, and shift the focus away from this true aim.

We are, however, aware that the linkage between biological sensors and the local environmental forcing is fundamental in any climate-proxy investigation. In the revised version of the manuscript, we have included results from an additional analysis we have performed to support

and improve the discussion on this that was already provided in our discussion paper on page 4445.

We explore the sensitivity to noise by proposing a series of idealized pseudo-proxy experiments, where different levels of white and red noise (following von Storch et al., 2009) are added to the original predictors' series in the validation period. We plan to report the results in an additional supplementary figure, which is shown below. It is clear that the reconstruction skills are most sensitive to the level of noise introduced rather than the type of noise, at least for when the relative amount of noise introduced remains low. For a signal-to-noise ratio of 1 (Figure S13c,f), most reconstructions are unskillful for the case of red noise and skillful for the white noise, although in both cases the explained variance for the validation period never reaches the 50% level. Some skills remain for signal-to-noise ratio larger than one.



New supplementary Figure S13 – Skill metrics for an ensemble of TT2010-like reconstructions following Figure 7b but highlighting the impact of predictors' noise on the pseudo-reconstructions. Different panels illustrate results from different types and levels of noise, which is only added for the validation period. Top: white noise; bottom: red noise; noise contributes to 10% (a,d), 25% (b,e) and 50% (c,f) of the predictors' total variance. Results are for 1000 pseudo-reconstructions without pre-selection of predictors based on calibration skills. The numbers inside each panel indicate the minimum and maximum R^2_v values obtained for each model. Insets in each panel map the three boxes from where gridded data are sampled to be included as predictors, with the name reported in each box (tas: surface air temperature, pr: precipitation). Red noise is assumed to be an autoregressive lag-1 process, generated following von Storch et al. (2009). Specifically, the value of the lag-1 autocorrelation is drawn at random from a beta distribution (parameters 7 and 3), in the interval (0,1).

Ref.: von Storch, H., E. Zorita, F. González-Rouco (2009) Assessment of three temperature reconstruction methods in the virtual reality of a climate simulation. *Int. J. Earth. Sci. (Geol Rundsch)* 98:67–82, doi:10.1007/s00531-008-0349-5

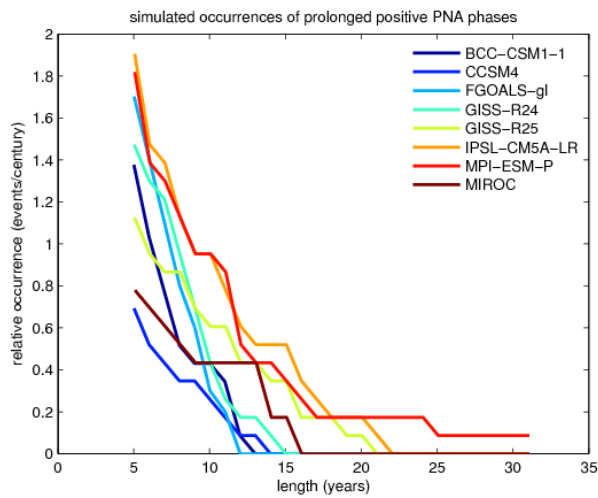
Pg. 4436: *It would be useful for the authors to consider the stationarity of the PNA teleconnection pattern to both temperature and precipitation. Related studies that have looked at the stationarity of the ENSO teleconnection pattern to North America have found that the PMIP3 LM simulations are characterized by a widely varying range in the temporal character and strength of the teleconnection (Coats et al., GRL, 2013). Similar results for the PNA would have implications for the interpretation of the pseudo-proxy reconstructions and model-data comparisons that the authors perform.*

We agree that non-stationarity of teleconnections is a possible important factor to take into account. This was already mentioned in the original discussion paper based on work by, e.g., Raible et al. (2014). The temporally varying R^2 skills of the pseudo-reconstructions in Figure 8 can also be interpreted as reflecting the non-stationarity of teleconnections. In the revised version of the manuscript, we have shortly expanded the discussion in the manuscript based on results by Coats et al. (2013). However, following on our reply to the previous point, adding such a factor in our analysis would add quite some complexity, and possibly the outcome would be lowering the skills while adding uncertainty to the reconstructions, i.e., again shifting focus away from our scope to delineate the upper bound of this reconstruction method.

Pg. 4438, Ln. 20: *The PNA is dominant over which collection of modes considered?* Over the four modes we considered (PNA, NPI, ENSO, NAO). We have specified this in that portion of the text.

A final point is necessary regarding the authors' argument about internal variability. I do not take issue with their interpretation, but it also appears that the models never produce a period of consistently positive PNA values as evidenced in the PNA reconstruction. They might consider asking whether any of the models produce periods of such positive excursions (in magnitude and/or extent), regardless of their timing. If indeed the persistently positive anomalies are a part of internal variability, they should occur at some other time in the simulation (or in the control simulations). If they do not occur, then perhaps there is more of a fundamental disagreement between the models and the reconstructions that is either the result of model failures or reconstruction uncertainties. The authors may wish to consider a similar analytical approach as outlined in Coats et al. (J. Clim., 2015), who similarly evaluated the ability of the PMIP3 models to produce multidecadal drought periods in the American SW in LM and control simulations.

This issue was meant to be addressed with Figure 9, which focus on interdecadal positive PNA phases (i.e., positive phases with duration comparable to that of the reconstructed PNA during the early 19th century) detected along all simulations, regardless of their timing. In the revised version of the manuscript, we have provided a modified Figure 4 which includes, in panel a, occurrences of prolonged periods of strong positive PNA. The modified figure shows that prolonged positive PNA periods occur along the whole integration period, and their occurrences are generally not consistent across the ensemble members. Furthermore, following the analysis by Coats et al. (2015), we have provided an additional supplementary figure (Figure S14, see below), showing the frequency of occurrence of prolonged positive PNA phases according to different durations. The figure shows that prolonged positive PNA periods longer than 20 years are extremely unlikely events in the ensemble. We have also added a short paragraph in the discussion about this, including reference to Coats et al., 2015.



New supplementary Figure S14 – Relative occurrences of prolonged positive PNA phases in the different simulations. An event of duration l is individuated when the standardized (with respect to the period 1725-1999) smoothed PNA index (11-year running mean) remains above the value of 1 for l consecutive years.

Technical Note: Many of the figures have *very* small axis labels, legend text, tick labels, titles, etc. I would strongly encourage the authors to think about improving these problems across all of the figures for better viewing and interpretability.

We have checked the figures for readability. We intend to “tune” again the aspect of the figures in this sense when it is clear how they will appear in their final published form, if the manuscript is accepted for publication in *Climate of the Past*.

Response to Reviewer #2

We thank the Reviewer for his/her appreciation of our work and appreciate his/her helpful comments. Below, we reply to his/her specific comments.

1. Pg. 4430. Ln. 23-25 Because the authors argue that volcanic activity can play a role in anomalous positive PNA values from early 19th century, an aspect not discussed in TT2010 paper, it would be useful at this point to have more information in the manuscript about the processes behind volcanic activity and PNA dynamics.

Reply: The possible link between volcanic eruptions and the PNA was briefly mentioned in the introduction (page 4428, lines 9-12). In section 2.1 of the revised manuscript, we refer to Li et al. (2013) and Zanchettin et al. (2014) for details on possible mechanisms underlying this link.

2. Pg. 4430. Ln. 20-25. It is argued that anomalous long period of positive PNA index during early 19th century could be related to both low solar activity (Dalton minimum) and strong volcanic activity. Is this coincidence unique in the observational and simulated periods considered in this study?

Reply: No, the coincidence is not unique: reconstructions of solar and volcanic forcing for the last millennium suggest that volcanic clusters also occurred during other periods of weak solar activity (e.g., mid 15th century). We briefly mention this in the discussion of the revised manuscript by adding the following sentence: “Further supporting this hypothesis, the simulations ensemble does not point to coherent positive PNA anomalies during other periods of the last millennium with concomitant strong volcanic forcing and weak solar forcing, e.g., the mid 15th century and the late 17th century (Figure 4a).”

3. Pg. 4432. Ln. 1-5. Usually the anomaly centers of teleconnection patterns in model simulations are located in different positions, according to model characteristics. Therefore is better to define the PNA index according to model characteristics, usually through an EOF analysis of Z500 in the Pacific North American sector. Is the PNA the dominant pattern of Z500 winter variability in the Pacific North American sector in the model simulations? Furthermore, are the results presented in the paper sensitive to the definition of the PNA index?

Reply: We agree with the Reviewer that centers of action of climate variability modes in climate simulations are sometimes displaced compared to observations. Our choice to use the modified pointwise method for PNA calculation stems from the need to base the pseudo-proxy analyses on an index that is independent of the temporal domain considered for its construction. EOF-based indices are, instead, dependent on the chosen temporal domain.

Furthermore, if PNA centers are displaced in a model, we should then accordingly modify the regions used in that model to sample predictors for the pseudo-reconstruction experiments. Therefore, using an EOF-based PNA index would complicate the

interpretation of our results on several levels. Besides, our definition allows for a straightforward description of models' skills in reproducing observed PNA features. We nonetheless recognize the importance to assess, at least briefly as done here, the differences between PNA indices in order to increase confidence in our conclusions. We added supplement Table S1 to the revised manuscript, which provides a comparison between PNA indices calculated based on the modified pointwise method (mpm, as originally used in this study) and on EOF analysis.

It is difficult to individuate the PNA pattern consistently across models as given EOF or rotated EOF based on northern hemispheric 500 hPa geopotential heights (Z500), so we focus on the Pacific/North American domain (0-90°N: 120-300°E) and define a PNA index for the observational period as the principal component of the first EOF of DJF Z500 over such domain. The results indicate overall highly significant correlations between the mpm-based and EOF-based PNA indices. The correlation is strongest for reanalyzed indices that are practically undistinguishable (see caption of Table S1). In the following, we provide more detailed information about the comparison, which we do not include in the revised manuscript. Spatial correlations between simulated and reanalyzed northern hemispheric patterns of EOF-based PNA indices vary quite remarkably across the simulations, similarly to what was diagnosed for the mpm-based indices. The quality of the EOF-based PNA pattern worsens for FGOALS-g1 compared to the mpm-based pattern, due particularly to a ~20° westward displacement of the negative center over the subtropical western Atlantic (a similar issue affects also MIROC-ESM). The EOF-based PNA patterns of both GISS-E2-R simulations worsen compared to the corresponding mpm-based patterns, as the hemispheric imprint in the former incorporates features of the annular mode. Patterns remain overall unchanged for BCC-CSM1-1, CCSM4 and especially IPSL-CM5A-LR and MPI-ESM-P.

We have summarized the above in the following paragraph, which has been added to section 4 of the revised manuscript:

“Our definition of the PNA index does not account for possible displacements of its centers of actions in simulated patterns compared to reanalyses. An alternative definition based on empirical orthogonal functions (EOF) results in PNA indices that share between half (MIROC-ESM) and almost the whole (CCSM4) total variance with the pointwise-based PNA indices over the observational period (see supplementary Table S1). Spatial differences between simulated EOF-based and pointwise-based patterns also vary considerably across the ensemble (Table S1). It is not yet clear whether and how these uncertainties related to the index definition affect the details of the pseudo-reconstructions. The validity of our general conclusions clearly stands for the sub-ensemble including only models with the most consistent PNA indices across the two definitions (CCSM4, IPSL-CM5A-LR, MPI-ESM-P).”

4. Pg. 4433. Ln. 17-19. Please define clearly the three regions over the North America used for pseudo-reconstructions.

Reply: done (see changes in section 2.1 of revised manuscript).

5. Pg. 4435, Ln. 9-10. It is expected to have a PNA like structure in all models

due to the definition of the PNA index. An EOF analysis of Z500 in the Pacific North American region would confirm better if the PNA structure is captured or not in the model simulations.

Reply: see our reply to comment 3.

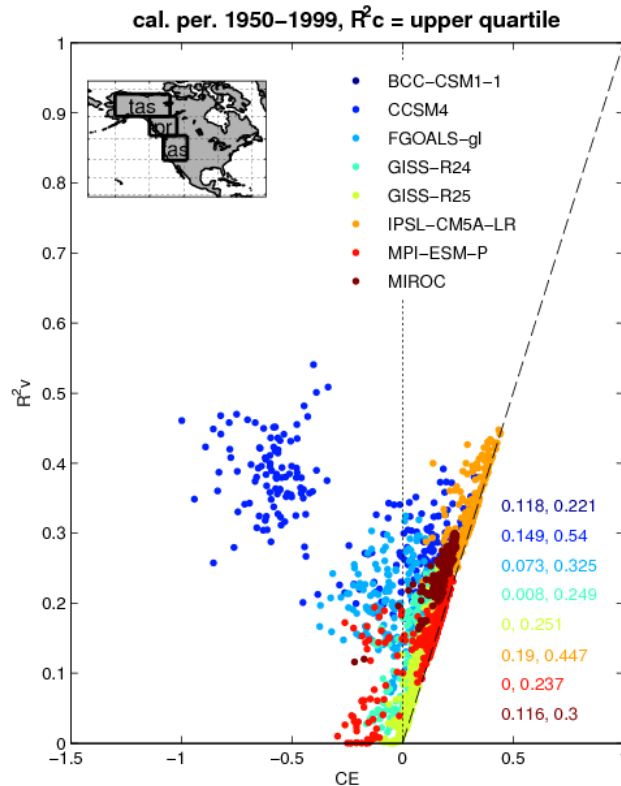
6. Pg. 4437. The paper is focused on TT2010 PNA reconstruction which is based on three tree ring records. As the relationship between tree ring variability and climate forcing present strong seasonal characteristics, would be interesting to see if significant simulated temperature or precipitation anomalies are recorded over northwestern North America during early 19th century not only in winter (Fig. S11) but also in other seasons. The TT2010 tree rings records are significantly correlated with temperature and precipitation not only from winter but also from other seasons. In fact the highest correlation is obtained for MTE tree ring record and summer temperature (Fig. 2 from TT2010). Therefore the anomalous reconstructed PNA values during early 19th century could reflect also the autumn, spring or summer temperature or precipitation anomalies from the northwestern North America.

Reply: as we stated on page 4434 of the originally submitted manuscript, we detect the strongest signals in winter temperature and precipitation. As we stated in the manuscript, the latter are needed to be included as predictors in order to obtain calibration skills comparable to the original reconstruction by Trouet and Taylor (2010).

The best skills (in analogy with Figure 7b) of a pseudo-reconstructions obtained using winter temperature for the Alaska box, winter precipitation for the Montana box, and summer temperature for the Wyoming box (a setting reflecting the strongest correlations in Figure 2 of Trouet and Taylor, 2010) are presented in the figure below. Many of the so-obtained pseudo-reconstructions are not skillful, with only a few of them exceeding the R^2 value of 0.4. Calibration skills are similarly below the scores obtained by Trouet and Taylor (2010).

We have added in the revised manuscript the following sentence in section 2.3:

“In particular, reconstruction skills considerably degrade if the predictor for “Wyoming” is defined as summer temperature instead of winter temperature (see section 2.1).”



Above – Same as Figure 7b of the main manuscript but using winter temperature for the Alaska box, winter precipitation for the Montana box, and summer temperature for the Wyoming box as predictors.

7. Pg. 4436: It would be useful to investigate systematically the stability of the correlation of the PNA index and temperature and precipitation from model grid points over northwestern North America by drawing running correlation curves similar to those represented in Figure 5 for climate indices. Selection of the temperature and precipitation anomalies from the grid-points where the correlation is stable, according to a certain stability criteria, as predictors could lead to an improvement of PNA reconstruction.

Reply: this would be an interesting exercise, but beyond the scope of this study, whose aim is to determine how reliable the pseudo-reconstructions are based on selection of proxies only from the observational period (the only period when in reality calibration is feasible). Nonetheless, the results presented in Figure 7c partly respond to the question raised by the Reviewer: the reconstruction skills improve if information from a longer period is used to calibrate the model (i.e., more stable predictors are selected).

8. Pg. 4438. It would be useful to give some hints related to physical processes that explain the negative correlation between PNA and NAO in most of the simulations (Fig. 5b).

Reply: We have included the following statement in section 3.2 referring to Figure 5:

“The negative PNA-NAO correlations represent periods when the atmospheric bridge linking Pacific and Atlantic climate variability is active (for a dynamical description see, e.g., Raible et al. 2001; Pinto et al., 2010; Baxter and Nigam, 2013). Decadal active phases of such bridge in the form of persistent negative PNA/positive NAO pattern have been attributed to both, internal variability (Pinto et al., 2010) and strong volcanic forcing (Zanchettin et al., 2012).”

Technical notes

1. Pg. 4428. Ln, 19. Please correct the period of Dalton minimum (_ 1790-1830)

Reply: Done, thanks

2. The labels of the axis from most of the figures are too small. Also there are many curves on the same figure and is difficult to identify them only by color.

Reply: We checked all figures for readability, and will be available to tune their format further for best appearance in the published version, if the manuscript is accepted.

1 *Reconciling reconstructed and simulated features of the winter Pacific-North-*
2 *American pattern in the early 19th century*

3
4 Davide Zanchettin^{1,2*}, Oliver ~~Bothe~~³, Flavio ~~Lehner~~^{4†}, Pablo ~~Ortega~~⁵, Christoph C.
5 ~~Raible~~⁴, and Didier ~~Swingedouw~~⁶

Deleted: Bothe²

Deleted: Lehner³

Deleted: Ortega⁴

Deleted: Raible³

Deleted: Swingedouw⁵

6
7 ¹Max Planck Institute for Meteorology, Bundesstrasse 53, 20146 Hamburg, Germany

8 ~~²University of Venice, Dept. of Environmental Sciences, Informatics and Statistics, Calle Larga Santa~~
9 ~~Marta, Dorsoduro 2137, 30123 Venice, Italy~~

Formatted: Superscript

Formatted: English (U.S.)

10 ~~³HZG, Helmholtz Center Geesthacht, Max Planck Strasse 1, 21502 Geesthacht, Germany~~

Deleted: ³HZG

Formatted: Italian (Italy)

11 ~~⁴Climate and Environmental Physics Institute and Oeschger Centre for Climate Change Research,~~
12 ~~University of Bern, Sidlerstrasse 5, 3012 Bern, Switzerland~~

Deleted: ³Climate

13 ~~⁵LOCEAN-IPSL/UPMC, 4, place Jussieu, Paris, France~~

Deleted: ⁴LOCEAN

Formatted: French (France)

14 ~~⁶UMR CNRS 5805 EPOC - OASU - Université de Bordeaux, Allée Geoffroy St Hilaire, 33615 Pessac~~
15 ~~cedex, France~~

Deleted: ⁵UMR

16 * corresponding author: davide.zanchettin@mpimet.mpg.de

17 ~~[†]currently at National Center for Atmospheric Research, Boulder, USA~~

Formatted: Font: 10 pt

18
19 **Abstract**

20 Reconstructions of past climate behavior often describe prominent anomalous periods
21 that are not necessarily captured in climate simulations. Here, we illustrate the contrast
22 between an interdecadal strong positive phase of the winter Pacific/North American
23 pattern (PNA) in the early 19th century that is described by a PNA reconstruction based
24 on tree-rings from northwestern North America, and a slight tendency towards negative
25 winter PNA anomalies during the same period in an ensemble of state-of-the-art coupled
26 climate simulations. Additionally, a pseudo-proxy investigation with the same simulation
27 ensemble allows assessing the robustness of PNA reconstructions using solely
28 geophysical predictors from northwestern North America for the last millennium. The
29 reconstructed early-19th-century positive PNA anomaly emerges as a potentially reliable
30 feature, although ~~the pseudo-reconstructions are~~ subject to a number of sources of
31 uncertainty and ~~deficiencies are highlighted especially at multidecadal and centennial~~
32 ~~timescales~~. The pseudo-reconstructions demonstrate that the early-19th-century

Deleted: it

Deleted: is

Deleted: potential

33 discrepancy between reconstructed and simulated PNA does not stem from the
34 reconstruction process. Instead, reconstructed and simulated features of the early-19th-
35 century PNA can be reconciled by interpreting the reconstructed evolution during this
36 time as an expression of internal climate variability, which is unlikely to be reproduced in
37 its exact temporal occurrence by a small ensemble of climate simulations. However, firm
38 attribution of the reconstructed PNA anomaly is hampered by known limitations and
39 deficiencies of coupled climate models and uncertainties in the early-19th-century
40 external forcing and background climate state.

Deleted: hence

Deleted: conditions

41

42 1. Introduction

43 The Pacific/North American pattern (PNA) is one of the dominant modes of interannual
44 winter atmospheric variability of the northern extratropics (*e.g.*, Barnston and Livezey
45 1987; Wallace and Gutzler, 1981). It strongly affects the weather and the hydroclimate of
46 the North American continent, and contributes to the atmospheric bridge linking Pacific
47 and Atlantic climate variability (*e.g.*, Raible et al. 2001; Pinto et al., 2010; Baxter and
48 Nigam, 2013). The behavior of this large-scale atmospheric circulation pattern before the
49 observational period and its sensitivity to natural external forcing are less understood
50 compared to other dominant climate modes, partly due to the limited number and
51 temporal coverage of available PNA reconstructions. In fact, only one major winter PNA
52 reconstruction, based on tree-rings from northwestern North America, is available and
53 only goes back to 1725 (Trouet and Taylor, 2010, hereafter: TT2010) (see section 2.1 for
54 details). Here, we investigate the PNA features described by a multi-model ensemble of
55 state-of-the-art climate simulations of the last millennium and use pseudo-proxy
56 experiments (*e.g.*, Lehner et al., 2012; Smerdon, 2012) applied to the same ensemble to
57 improve our understanding of the PNA's behavior during the pre-industrial period,
58 especially during the early 19th century, and to investigate compatibility between climate
59 simulations and reconstructions.

Deleted: clarify aspects of

Deleted: the

Deleted: rab

Deleted: of

Deleted: with

60 The PNA pattern consists of a wave train spanning from the subtropical northeastern
61 Pacific to the Gulf of Alaska, northwestern North America and the southeastern United
62 States through centers of action of alternating sign (Figure 1). Accordingly, a classical
63 definition of the PNA index is the sum of the differences between its positive and

64 negative centers of action (Wallace and Gutzler, 1981). The PNA can be interpreted as an
65 amplification and dampening of the climatological stationary wave characterizing the
66 pattern of the polar jet across North America (*e.g.*, Notaro et al., 2006), which explains its
67 reduced importance during boreal summer. The positive phase of the PNA includes an
68 anomalously deep Aleutian low and an enhanced ridge-trough pattern across North
69 America. It produces above-average temperatures over northwestern North America due
70 to the stronger ridge over the North American Rockies with associated northward
71 diversion of the westerly flow, and below-average temperatures and drier conditions
72 across the south-central and southeastern United States due to increased southward
73 penetration of cold Arctic air masses. The signature is reversed for the negative phase of
74 the PNA.

75 On sub-monthly timescales the PNA variability and predictability are largely determined
76 by internal dynamics of the mid-latitude atmosphere, while on longer timescales they are
77 most prominently controlled by forcing from sea-surface temperature (SST) signals from
78 the tropical Pacific (Younas and Tang, 2013). Horel and Wallace (1981) were the first ~~to~~
79 ~~identify~~ a connection between the PNA and the equatorial El Niño-Southern Oscillation
80 (ENSO). Since then, observational and modelling studies have revealed that boundary
81 conditions relevant for the PNA also include low-frequency SST signals in the extra-
82 tropical North Pacific (Yu and Zwiers, 2007; Yu et al., 2007), remote forcing from the
83 North Atlantic (Baxter and Nigam, 2013), and upstream conditions determined by the
84 East Asian jet (*e.g.*, Gong et al., 2007).

85 Climate simulations of the last millennium indicate increased likelihood of a significantly
86 weaker Aleutian low after strong tropical volcanic eruptions, suggesting that the PNA can
87 dynamically respond to volcanic forcing on interannual to decadal time scales
88 (Zanchettin et al., 2012; Wang et al., 2012). A connection between PNA variability and
89 natural forcing is also suggested by the TT2010 reconstruction, which shows a prolonged
90 strong positive phase of the PNA during the early 19th century. Indeed, this period was
91 characterized by a close succession of strong volcanic eruptions concomitant with a phase
92 of weak solar activity, both contributing to exceptionally cold climate conditions (Cole-
93 Dai et al., 2009). However, TT2010 attributed the early-19th-century anomalous PNA
94 phase to the decreased solar irradiance during the Dalton Minimum of solar activity (ca.

Deleted: who

Deleted: identified

Deleted: 1890

Deleted: 1920

95 | ~~1790-1830~~), without discussing possible implications from the concomitant volcanic
96 | cluster.

97 | The selection of proxy locations is crucial for the robustness and reliability of
98 | reconstructions of large-scale circulation modes (Lehner et al., 2012). Decadal-scale
99 | shifts in the centers of action of atmospheric modes like the North Atlantic Oscillation
100 | (NAO) or the PNA are associated with non-stationarities in the imprint of such
101 | teleconnection patterns on local precipitation and temperature (Raible et al. 2006; [Coats,
102 | et al., 2013](#); Moore et al. 2013; Raible et al., 2014). Accordingly, the ring-width response
103 | to atmospheric modes like the PNA and the NAO is spatially heterogeneous due to the
104 | complex causal chain linking climate modes, local environment and seasonal tree growth
105 | (St. George, 2014). Reflecting such heterogeneity, the prolonged positive PNA phase in
106 | the early 19th century becomes less prominent if proxies from other PNA-sensitive
107 | regions are considered, such as river catchments in western-central British Columbia
108 | (Starheim et al., 2013) or lakes from the north-eastern United States (Hubeny et al.,
109 | 2010).

110 | Twentieth-Century-Reanalysis data suggest that the PNA centers of action are less
111 | variable in space than, *e.g.*, the NAO (Raible et al. 2014). However, the risk of
112 | insufficient coverage and representation of its different centers of action – hence of poor
113 | reconstruction – is considerable for the PNA due to the complexity of its pattern and the
114 | strong interdependencies with surrounding or even superposing modes of variability. For
115 | instance, over the last six decades and especially in winter the PNA is practically
116 | indistinguishable from the inverted North Pacific Index (NPI) describing the sea-level
117 | pressure (SLP) variability in the Aleutian low region. However, there is no indication so
118 | far about whether the NPI and the PNA (and their signatures on regional temperature and
119 | precipitation) can become distinguishable over periods of decades or longer. Similarly,
120 | late-winter temperature reconstructions in western North America, *i.e.*, a region where
121 | the PNA climatic imprint is strong, have been recently used to test whether strong
122 | tropical volcanic eruptions induce a preferred phasing of ENSO (Wahl et al., 2014).
123 | [However, the simulated teleconnection between ENSO and North America climate is
124 | nonstationary on multidecadal timescales \(Coats et al., 2013\)](#). The possible superposition
125 | of regional climate signatures of different large-scale modes (like ENSO, PNA and NPI)

126 | and their possible nonstationarity poses a challenge for any reconstruction attempt using
127 | climate-proxies from affected regions, in particular to produce robust and unambiguous
128 | reconstructions. There is therefore a need to assess the robustness of proxy-based PNA
129 | reconstructions: If the TT2010 reconstruction was found to accurately capture the past
130 | PNA behavior, the reconstructed prolonged strong positive PNA phase during the early
131 | 19th century would represent an important feature to address in coupled climate
132 | simulations. Its robust reproduction by climate simulations would be strong evidence for
133 | its externally-driven nature, while the opposite would suggest two possibilities: either an
134 | episodic excitation consistent with internal variability, or limited realism of climate
135 | models due to common deficiencies.

Deleted:

136 | Thus, this study aims at answering the following questions: Is the reconstructed
137 | prolonged, strong positive PNA phase during the early 19th century reliable? What can
138 | we learn from available climate simulations of the last millennium about its attribution?
139 | To answer these questions we compare simulated and observed/reconstructed PNA
140 | features, and perform a series of pseudo-proxy experiments on a multi-model ensemble.
141 | We also extend our pseudo-proxy investigation to determine whether margins exist to
142 | substantially improve the PNA reconstruction.

143

144 | **2. Data and methods**

145 | *2.1 The TT2010 PNA reconstruction*

146 | The TT2010 reconstruction of the winter PNA covers the period 1725–1999. It is based
147 | on a multiple regression model using three winter climate sensitive tree-ring records from
148 | the western United States as predictors (TT2010). The predictors were sampled from
149 | three regions, whose location is marked by the green boxes in Figure 2 and that are
150 | hereafter referred to as “Alaska” (northern box, here defined as: [60-70]°N, [120-
151 | 160]°W), “Montana” (middle box, [50-60]°N, [115-135]°W) and “Wyoming” (southern
152 | box, [35-50]°N, 107.5-125°W), respectively. The Alaskan predictor is most sensitive to
153 | winter temperature, the predictor from Montana captures winter precipitation in a
154 | relatively high-elevation site whereas the predictor from Wyoming captures both
155 | autumn/winter precipitation and summer temperature in a relatively low-elevation, semi-
156 | arid site (TT2010). The latter two predictors show opposite sensitivity to precipitation

Deleted: first

Deleted: over Alaska

Deleted: .

Deleted: T

Deleted: second

Deleted: and third

Deleted: s

Formatted: Font: Bold

Deleted: er

Deleted: in Wyoming, and winter precipitation in a higher-elevation site in Montana, respectively

157 despite their close location, highlighting the role of regional topographical features in
158 determining the relationship between the biological sensor and the local environmental
159 conditions. The combination of the selected three tree-ring series explains 49 % of the
160 variance of the winter PNA index for the calibration period 1949-1999 (TT2010).

161 The TT2010 PNA reconstruction shows a prolonged period of positive PNA, with a peak
162 in 1800–1820. The early-19th-century positive PNA phase was interpreted as a response
163 to the decreased solar irradiance since it coincides with the period of weak solar activity
164 known as Dalton Minimum and since subsequent periods of weak solar activity similarly
165 correspond to positive PNA anomalies (TT2010). Radiatively forced warming of eastern
166 tropical Pacific SST associated with cold SST anomalies in the Aleutian Low region -
167 corresponding to an in-phase behavior between positive anomalies of both ENSO and the
168 Pacific Decadal Oscillation - was reported as a possible dynamical explanation for the
169 connection between decreased solar irradiance and positive PNA phase. TT2010 did not
170 discuss the possible implications of the strong volcanic eruptions during the early 19th
171 century. Possible mechanisms underlying volcanically-forced PNA variability include
172 both tropical-extratropical coupling via volcanically-forced changes of ENSO (e.g., Li et
173 al., 2013) and extratropical processes via, e.g., sea-ice responses in the Gulf of Alaska
174 and the Bering Strait region (e.g., Zanchettin et al., 2014).

Deleted: forcing

Formatted: Font: Italic

Formatted: Font: Italic

Formatted: Font: Italic

175

176 *2.2 Observational and simulated data*

177 We use monthly-mean data obtained from the NCEP reanalysis (Kalnay et al., 1996;
178 Kistler et al., 2001) for the period 1948-2013 as reference data for the observational
179 period. The data were provided by the NOAA/OAR/ESRL PSD, Boulder, Colorado,
180 USA. The NCEP reanalysis dataset suits our needs since it encompasses the calibration
181 period used in the TT2010 reconstruction. The Twentieth Century Reanalysis (Compo et
182 al., 2011) extends further back in time, but the ensemble teleconnection patterns over the
183 Pacific from this dataset are poorly constrained during the first half of the 20th century
184 (e.g., Raible et al., 2014).

185 We include outputs from the *past1000* and the follow-up *historical* climate simulations
186 from seven coupled general circulation and Earth system models contributing to the third
187 phase of the Paleoclimate Modelling Intercomparison Project (PMIP3, Braconnot et al.,

Deleted: earth

188 2012). All simulations are full-forcing simulations, *i.e.*, they describe the combined
189 effects of all major natural and anthropogenic external forcing factors acting during the
190 last millennium (Schmidt et al., 2013). Two simulations are considered for the GISS-E2-
191 R model (hereafter referred to as GISS-E2-R24 and GISS-E2-R25, respectively), which
192 differ in the considered external forcing inputs. Table 1 provides a summary of the main
193 characteristics of the models and simulations considered.

194 Bothe et al. (2013) provide an assessment of the probabilistic and climatological
195 consistency of the PMIP3-past1000 simulations relative to proxy-based reconstructions
196 under the paradigm of a statistically indistinguishable ensemble. They diagnose
197 distributional inconsistencies between ensemble-simulated surface-air temperatures and
198 the global temperature field reconstruction of Mann et al. (2009) over large areas of the
199 globe, including PNA-sensitive regions over North America (see their Figure 1). These
200 full-period inconsistencies originate mainly from differences in multicentennial to
201 millennial trends (Bothe et al., 2013). By contrast, the ensemble was found to be
202 probabilistically consistent with the reconstructed annual temperatures for the North
203 America Southwest since year 1500 (Wahl and Smerdon, 2012).

204

205 ***2.3 Indices and definitions***

206 The following indices and definitions are considered based on monthly-mean data:

- 207
- 208 • the PNA is calculated using the modified pointwise method currently adopted by
209 the NOAA-CPC and applied to 500 hPa geopotential height (Z500) data. The
210 index is defined as $Z^*_{[15-25^\circ\text{N}; 180-220^\circ\text{E}]} - Z^*_{[40-50^\circ\text{N}; 180-220^\circ\text{E}]} + Z^*_{[45-60^\circ\text{N}; 235-255^\circ\text{E}]} -$
211 $Z^*_{[25-35^\circ\text{N}; 270-290^\circ\text{E}]}$, where Z^* denotes monthly Z500 anomalies from the respective
212 climatological value, and the suffix [x] indicates spatial averaging over the
213 domain x. [We briefly discuss a different definition of the PNA index in section 4;](#)
 - 214 • the NAO index is calculated based on the latitude-longitude 2-box method by
215 Stephenson et al. (2006) applied on Z500 data, *i.e.*, as the pressure difference
216 between spatial averages over [20-55°N; 90°W-60°E] and [55-90°N; 90°W-60°E];
 - 217 • the NPI is calculated using the definition from Trenberth and Hurrell (1994)
applied to SLP data. The index is computed as the spatial SLP averaged over [30-

218 65°N; 160-220°E], so that positive phases of the index indicate a weaker-than-
219 normal Aleutian low and the opposite holds for the negative phases;

- 220 • the SOI is calculated based on a modified version of the Tahiti-Darwin index. It is
221 defined as the difference between the average SLP over the domains [20-15°S;
222 147-152°W] and [15-10°S; 128.5-133.5°E]. The SOI is here preferred to SST-
223 based ENSO indices since we focus on the atmospheric component of ENSO.

224 Indices are not standardized by default in order to highlight inter-model differences in the
225 climatology and in the amplitude of fluctuations associated with the indices.

226

227 ***2.4 Pseudo-proxy experiments***

228 Pseudo-proxy experiments are conducted to test the robustness and potential skills of
229 PNA reconstructions using solely geophysical predictors from northern North America.
230 Millennium-scale transient simulations from climate models provide a long and
231 physically consistent framework where paleoclimate reconstruction methods can be
232 altered and evaluated systematically in absence of the spatial and temporal discontinuities
233 of the real-world climate-proxy networks (Smerdon, 2012). In particular, they may allow
234 determining an upper limit in the accuracy of the reconstruction of large-scale modes
235 under limited spatial sampling.

236 Our pseudo-proxy experimental approach is meant as a generalization of the method used
237 in TT2010. Specifically, the reconstruction is based on a multi-linear least-square
238 regression model of general form: $y^t = \sum_{i=1:N} a_i x_i^t + y_0 + \varepsilon^t$, where y^t is the reconstructed
239 value at time step t , N is the number of predictors, a_i is the regression coefficient of the i^{th}
240 predictor x_i , y_0 is the intercept and ε^t is the residual at time step t . All data are normalized
241 based on the full period before the pseudo-proxy experiments are conducted.

242 Pseudo-reconstructions are performed as follows: first, the pool of candidate predictors
243 including temperature and precipitation data is determined by defining three regions over
244 North America. Then, an ensemble of predictor-sets is built by iteratively (up to 1000
245 times) and randomly sampling one grid-point data from each region. Finally, an ensemble
246 of PNA pseudo-reconstructions is obtained by using the built sets in a multi-linear
247 regression. So, the robustness of PNA pseudo-reconstructions with a TT2010-like design
248 is tested using predictor sets that mimic the quality of the TT2010 reconstruction.

Formatted: Font: Italic

249 Accordingly, we consider only pseudo-reconstructions with R^2 skill metric in the range
250 between 0.45 and 0.55 for the calibration period (R^2_c), *i.e.*, the selection is based on
251 calibration skills instead of on a preliminary screening of climate proxies.

252 We follow a perfect-model approach with noise-free predictors, and the considered range
253 of R^2_c is meant to account for the possible effects of noise in the actual climate proxies.

254 The inclusion of noise in the predictors and its influence on the results are briefly
255 investigated with a series of pseudo-proxy experiments where predictors are artificially
256 perturbed by different types and levels of noise (section 4). Skill metrics calculated for

257 such noise-free predictor sets and regression models, but using other climate indices as
258 validation target instead of the PNA, clarify whether these pseudo-reconstructions
259 distinguish the PNA from other modes influencing North American regional climates.

260 Additionally, the PNA pseudo-reconstructions pertaining to the upper quartile of R^2_c for
261 each simulation provide a crude estimate of the quality of PNA reconstructions
262 obtainable with a TT2010-like method for the given set of sampling regions. An
263 exemplary different set of regions is also considered in the same reconstruction approach
264 to assess whether regions not included in the TT2010 design may allow for a notable
265 improvement in the accuracy and robustness of PNA reconstructions.

266 Skill metrics include R^2 and coefficient of error (CE) (Cook et al., 1994). CE is defined
267 as $[1 - \sum_{t=1:M}(x_t - y_t)^2 / \sum_{t=1:M}(x_t - x_{mv})^2]$, where x_t and y_t are the observed and the predicted
268 index in year t , respectively. x_{mv} is the observed mean index over the validation period
269 and M is the number of years in the validation period. R^2 values are also calculated for
270 successive 30-year periods to highlight the robustness of the pseudo-reconstructions over
271 different interdecadal periods.

272 Unlike in TT2010, the predictors sampled herein from the “Montana” (middle) and
273 “Wyoming” (southern) boxes are winter temperature and precipitation, respectively. This

Deleted: lower

274 choice guarantees that our pseudo-reconstructions encompass the desired R^2_c range in all
275 models, which is hardly achieved for pseudo-proxies from these regions following the
276 original definition. In particular, reconstruction skills considerably degrade if the

277 predictor for “Wyoming” is defined as summer temperature instead of winter temperature
278 (see section 2.1). This does not affect the generality of our conclusions, since we aim at

Deleted:

279 testing PNA reconstructions based solely on local geophysical predictors from

280 northwestern North America, not at replicating the linkage between biological sensors
281 and the local environmental forcing at the basis of the TT2010 reconstruction.
282 ~~All the following analyses are performed using winter-average (DJF) data and using~~
283 1950-1999 as the calibration period, unless specified otherwise. Furthermore, unless
284 specified otherwise, the validation period is defined as the period spanning from the
285 beginning of the simulation to the last year before the calibration period. The use of
286 unsmoothed data limits the effect of high autocorrelation leading to spurious high skills
287 metrics (Macias-Fauria et al., 2012).

Deleted:

Deleted: Thus, a

288

289 **3. Results**

290 ***3.1 Simulated PNA during the observational period***

291 First, we assess whether the employed models/simulations represent the
292 observed/reanalyzed dominant large-scale circulation and associated surface-air
293 temperature and precipitation patterns with sufficient accuracy for the observational
294 period. This comparison guarantees that they are suitable for the subsequent analyses.

295 The four centers of the observed PNA wave-pattern are generally well captured by the
296 simulations (Figure 1). A number of simulations, and most noticeably GISS-R24/-R25
297 (Figure 1e,f), display a weaker tropical center in the Pacific suggesting a weaker
298 connection between tropics and extra-tropics. Higher model resolution does not
299 systematically improve the overall quality of the hemispheric pattern. For instance, the
300 PNA imprint over the Arctic as well as the Pacific-Atlantic teleconnection are too strong
301 in the highly-resolved CCSM4 (Figure 1c). The PNA pattern of the lowest-resolution
302 model (FGOALS-g1) has an overall weaker hemispheric imprint and the negative center
303 over Florida is displaced westward over Mexico (Figure 1d), possibly reflecting an
304 inadequate representation of the Rocky Mountains.

305 A similar behavior is found for the simulated spatial patterns of NPI (see supplementary
306 Figure S1). Most noticeably, the NPI pattern in FGOALS-g1 includes strong negative
307 correlations over Central North America, again pointing to low-resolution topographic
308 issues. All simulations show a good representation of the NAO pattern over the North
309 Atlantic/Europe and China, but often overestimate its signature over the North Pacific
310 (Figure S2). The simulation of the SOI pattern is a challenge for most of the models,

311 especially concerning its signature over the extra-tropical North Pacific and North
312 America (Figure S3).

313 Our pseudo-reconstruction approach also requires that simulations produce reliable
314 imprints of the PNA - as well as of NPI, SOI and NAO - on North American winter
315 surface-air temperature and precipitation (Figures 2 and 3). The observed correlation
316 pattern between PNA and continental temperature is characterized by an approximately
317 meridional stretch of positive correlations along the eastern coast of the Pacific Ocean,
318 which extends eastward into continental regions at mid to polar latitudes, and by a center
319 of negative correlation over the Sargasso Sea/Florida (Figure 2a). Simulations capture
320 both features with varying quality (Figure 2b-i). For instance, the Sargasso Sea/Florida
321 center is displaced in BCC-CSM1-1 and FGOALS-g1, while it is underrepresented in
322 GISS-E2-R25, IPSL-CM5A-LR and slightly so in MIROC-ESM. Overall, FGOALS-g1
323 features the worst representation of this correlation pattern possibly due to the
324 deficiencies noticed above in the 500 hPa PNA pattern. Similar conclusions can be drawn
325 about the NPI signature on winter North American temperatures (Figure S4). Simulations
326 and reanalyses consistently point to a limited imprint of NAO and SOI on winter North
327 American temperatures (Figures S5 and S6), which for both modes partly superposes
328 with PNA signals.

329 Similar considerations could be derived for winter precipitation, but correlation patterns
330 between large-scale circulation modes and precipitation over land are patchier than for
331 temperature. Overall, the quality of simulated precipitation patterns compared to
332 reanalyses is clearly poorer than for temperature. Both reanalyses and simulations
333 indicate locally significant negative correlations between PNA and precipitation in the
334 mid-latitude United States (*i.e.*, wetter conditions under negative PNA, and *vice versa*),
335 but with substantial differences in the details of the pattern (Figure 3). An important
336 robust feature is that all simulations except GISS-E2-R25 indicate weak negative
337 correlations over the central Rocky Mountains (Figure 3b-i), a region where
338 precipitation-sensitive proxies were screened for the TT2010 reconstruction.

339 In summary, the correlation patterns reveal a marked heterogeneity between simulations
340 in the quality of their representation of dominant large-scale circulation modes and
341 associated imprint on the North American climate. Of course, the spatial patterns are

342 derived from the chosen 50-year period within single transient simulations, and are
343 therefore not necessarily representative of the quality of the different models. Still, some
344 general features are recognizable: A coarsely resolved North American topography and a
345 poor representation of tropical and extra-tropical Pacific interactions are likely two major
346 challenges limiting the quality of the simulated PNA imprints. The most apparent issues
347 concern FGOALS-g1, potentially due to its coarser resolution compared to the other
348 models.

349

350 ***3.2 Simulated PNA features during the last millennium***

351 The evolution of the winter PNA index throughout the last millennium shares little
352 resemblance between the different simulations (Figure 4a), which is indicative of a
353 limited effect of the external forcing since the latter is very similar across the ensemble.
354 Decadal and interdecadal phases of strong positive or, similarly, strong negative PNA
355 appear at different periods in different simulations, suggesting that, in general, the PNA is
356 mostly determined by internal variability at these time scales. No simulation displays a
357 prolonged strong positive PNA phase during the early 19th century as featured by the
358 TT2010 reconstruction, but decadal-scale positive PNA anomalies of similar relative
359 amplitude emerge sporadically in the ensemble during different periods (see dots in
360 Figure 4a). ~~Such prolonged positive-PNA events are, however, rare.~~ Unlike in the
361 reconstruction, the early 19th century is characterized by predominant negative PNA
362 trends in the simulations (the period of discrepancy is highlighted by a horizontal red bar
363 in Figure 4b).

364 Running-window correlations between the PNA index and the other indices provide a
365 simple assessment of the variable strength of PNA teleconnections in the different
366 simulations. Reanalysis data indicate that winter PNA and NPI are practically
367 indistinguishable: the two indices are robustly highly anti-correlated (thick black line in
368 Figure 5a). Simulations consistently feature significant negative PNA-NPI correlations
369 through the last millennium, although with considerable differences within the ensemble
370 concerning strength and stationarity of the statistics (Figure 5a). CCSM4 produces the
371 strongest and most robust correlations, which overlap with values from reanalyses,
372 whereas FGOALS-g1 produces the weakest and most time-varying correlations. The

Deleted: ,b

373 simulated winter PNA-NAO correlations are generally weak and negative during the last
374 millennium, in agreement with the non-significant and strongly varying statistics from
375 reanalysis data (Figure 5b). Some simulations feature multidecadal periods when the
376 negative correlation becomes statistically significant, suggestive of a temporarily strong
377 atmospheric connection between North Pacific and North Atlantic sectors. This is
378 especially the case for CCSM4 (compare also superposing patterns in Figure 1c and
379 Figure S2c). The negative PNA-NAO correlations represent periods when the
380 atmospheric bridge linking Pacific and Atlantic climate variability is active (for a
381 dynamical description see, e.g., Raible et al. 2001; Pinto et al., 2010; Baxter and Nigam,
382 2013). Decadal active phases of such bridge in the form of persistent negative
383 PNA/positive NAO pattern have been attributed to both, internal variability (Pinto et al.,
384 2010) and strong volcanic forcing (Zanchettin et al., 2012). The winter PNA-SOI
385 correlation is significantly negative in the reanalyses, though not very strong (Figure 5c).
386 CCSM4 produces PNA-SOI correlations that remain robustly around this observed value
387 throughout the last millennium, while the other simulations produce generally lower and
388 more variable correlations (Figure 5c). In BCC-CSM1-1, MPI-ESM-P and MIROC
389 correlations between SOI and both PNA and NPI (the latter not shown) are only
390 sporadically significant, meaning that these models feature a weak connection between
391 tropical and extra-tropical North Pacific. Note that these results do not qualitatively
392 change if running-window correlations are calculated over longer periods.
393 Changes in the relative importance of large-scale modes for North American winter
394 climate variability during the last millennium are assessed by comparing the fractional
395 variances of North American surface-air temperature and precipitation that are explained
396 by the different indices over sliding 30-year periods paced at one-decade intervals. The
397 winter PNA is the dominant mode of simulated North American winter temperature
398 variability among the considered indices (PNA, NPI, ENSO), generally explaining
399 around 20% of the total variance (Figure 6). Only for FGOALS-g1 there are several
400 periods when the NPI becomes more dominant than the PNA. The strength of all index
401 signatures changes through time. The fraction of North American winter precipitation
402 variability explained by the indices is generally below 10%, and the dominance of PNA
403 over the other indices is less clear than for temperature (Figure S7).

404 In summary, internal variability is an important factor for the simulated PNA during the
405 pre-industrial millennium. The ensemble markedly disagrees with the TT2010
406 reconstruction, whose strong positive phase in the early 19th century was interpreted as
407 resulting from a strong PNA response to solar forcing (TT2010). Correlations between
408 indices reveal substantial differences in the simulated representation of teleconnections
409 both within the ensemble and in comparison to reanalyses. Among the considered
410 indices, PNA generally explains the largest fraction of North American winter
411 temperature variability. Only FGOALS-g1 features prolonged periods when PNA and
412 NPI explain comparable fractions of North American winter temperature variability. We
413 are therefore confident that through proper sampling of precipitation and especially
414 temperature proxies over North America, pseudo-reconstructions are able to express
415 robust PNA signals rather than signals from other indices.

416

417 ***3.3 PNA pseudo-reconstructions***

418 First, we validate the reconstruction approach in TT2010. This is done in a perfect model
419 framework by testing whether a reconstruction design based solely on geophysical
420 predictors from northwestern North America can provide meaningful pseudo-
421 reconstructions of the PNA. We use only predictor sets that provide a calibration skill
422 comparable to that of the actual TT2010 reconstruction (Figure S8 summarizes the full-
423 ensemble of pseudo-reconstruction calibration skills).

424 The so-obtained PNA pseudo-reconstructions are generally skillful according to both
425 employed full-validation metrics (R^2_v and CE): only a few pseudo-reconstructions give
426 CE values below 0, meaning they have no predictive skill and are hence unacceptable
427 (Figure 7a). R^2_v values can exceed the imposed R^2_c range (see columns of numbers in
428 Figure 7a). In some simulations, different performance between the validation and
429 calibration periods can be related to the presence of significant local trends in North
430 American winter temperatures during the latter period (Figure S9) that are mostly due to
431 strong anthropogenic forcing imposed in the second half of the 20th century. For some
432 simulations and predictor sets, the validation-period R^2 values (R^2_v) for the PNA overlap
433 with those from the NPI (Figure S10), meaning that in these cases the pseudo-

434 reconstructions are hardly effective in distinguishing PNA-related features from other
435 signals.

436 The robustness of a reconstruction through time is a major concern for its reliability.
437 Figure 8 shows that for the same set of predictors used for Figure 7a the R^2 skill of the
438 pseudo-reconstructions changes remarkably through time: There are periods when the
439 pseudo-reconstructions from one simulation are consistently poorer, other periods when
440 they are consistently better, and there is generally a large spread in the quality of the
441 pseudo-reconstructions. The multidecadal and centennial variations of R^2 suggest that
442 there is structural uncertainty on these time scales. Note that, since metrics are calculated
443 based on deviations from the 30-year average, the so-defined R^2 describes the
444 reconstruction skills mostly on interannual to decadal variability. The CE metric, which
445 accounts for the 30-year mean state, is characterized by non-stationarity and inter-model
446 spread similar to R^2 (not shown). Running-window statistics further indicate that the
447 models substantially differ concerning the comparative skills of reconstructed indices
448 (top panel of Figure 8): in some models, and most noticeably in GISS-E2-R, the skills for
449 the PNA are often not better than for NPI; in other models, like MPI-ESM-P and BCC-
450 CSM1-1, the skills for the PNA are better than for all other indices. We conclude that the
451 approach is effective in distinguishing the reconstructed PNA from other indices only for
452 the latter models.

453 Another of our main objectives is to assess the robustness of the interdecadal strong
454 positive PNA phase identified by the TT2010 reconstruction in the early 19th century.
455 Figure 8 shows particularly large inter-model spread in the R^2 metric during the late 18th
456 and early 19th centuries, with some simulations performing very well (IPSL-CM5A-LR,
457 GISS-E2-R25 and MPI-ESM-P) while others show some of the poorest skills in the entire
458 millennium (*e.g.*, BCC-CSM1-1 and GISS-E2-R25). It should be noted that the PNA
459 pseudo-reconstructions are generally biased towards negative PNA values (black vertical
460 lines in Figure 9). This is mainly due to the fact that most simulations have strong local
461 trends in 20th century temperatures (Figure S9), which result in PNA pseudo-
462 reconstructions roughly following a hockey-stick shape over the last millennium. As a
463 consequence of this bias, our pseudo-reconstructions tend to underestimate interdecadal
464 | phases of very strong positive PNA [that are detected throughout the simulations](#) (see the

465 negatively-centered histogram in Figure 9a). By contrast, interdecadal phases of strong
466 positive PNA in the pseudo-reconstructions seem to describe the actual PNA conditions
467 more accurately, as shown by the rather symmetric, almost zero-centered probability
468 distribution of ensemble residuals for these events (Figure 9b). So, whereas actually
469 simulated prolonged strong positive PNA phases may not be correctly captured by
470 pseudo-reconstructions, prolonged strong positive phases emerging in the pseudo-
471 reconstructions are generally ‘true’.

472 There are further concerns about the capability of pseudo-reconstructions to accurately
473 capture the PNA low-frequency variability. We find that pseudo-reconstructions tend to
474 overestimate the amplitude of multidecadal-to-centennial fluctuations (Figure 10). In
475 some simulations, like BCC-CSM1-1, CCSM4, FGOALS-g1 and MPI-ESM-P, the
476 spectra of the pseudo-reconstructions entail large-amplitude peaks in this frequency band
477 that do not appear in the spectrum of the actual index. GISS-E2-R and MIROC, by
478 contrast, produce pseudo-reconstructions whose spectra agree fairly well with that of the
479 simulated PNA. The different agreement between pseudo-reconstruction-spectra and the
480 actual PNA spectrum implies that the models disagree about whether i) the low-
481 frequency temperature and precipitation excursions captured by the pseudo-proxies are
482 related to the PNA and/or whether ii) the PNA reacts to the same low-frequency forcing
483 as the temperature and precipitation pseudo-proxies do. Combining evidence from
484 Figures 8, 9 and 10, we conclude that the errors in the pseudo-reconstructed prolonged
485 positive PNA phases and, more generally, the variable skills of pseudo-reconstructions on
486 multidecadal and centennial time scales reflect misrepresentation of low-frequency PNA
487 variability by the pseudo-reconstructions. This casts doubt on the reliability of the early-
488 19th-century PNA event identified by the TT2010 reconstruction.

489 Considering PNA pseudo-reconstructions instead of the actually simulated PNA indices
490 does not solve the discrepancy between simulations and the TT2010 reconstruction
491 during the early 19th century (Figure 4c). In fact, none of the simulations displays
492 significant positive winter temperature anomalies over northwestern North America
493 during the period 1800-1820 (Figure S11), which would be consistent with a positive
494 phase in the PNA pseudo-reconstructions following the current definition. Instead, the

495 anomalous patterns are characterized by a marked heterogeneity, suggesting lack of a
496 robust response to external forcing across the models, with no pattern resembling the
497 typical PNA structure. Accepting the reconstructed PNA behavior during the early 19th
498 century as accurate and the simulated climates as realistic, the apparent discrepancy can
499 only be solved by interpreting the first as a particular event of internal climate variability,
500 hence unlikely captured (in its temporal occurrence) in a small-size ensemble as the one
501 at hand. Indeed, a similar discrepancy is found in the late 1940s for a reconstructed
502 decadal-scale negative PNA phase (Figure 4c), a period not characterized by prominent
503 (inter)decadal forcing events.

504

505 **3.4 Designing new PNA reconstructions**

506 A natural question at this point is whether there is margin to improve reconstructions of
507 the PNA. Potential for improvement may come, for instance, from the inclusion of new
508 and/or better predictors over northwestern North America. Simulations disagree about
509 whether the skills of the actual TT2010 PNA reconstruction and of its synthetic analogs
510 represent the limit of this reconstruction approach: Some simulations (*e.g.*, BCC-CSM1-
511 1, FGOALS-gl) indicate that the calibration skill of the TT2010 reconstructions is close
512 to the expectation for the method (Figure S8). In other simulations, including CCSM4
513 and IPSL-CM5A-LR, geophysical predictor sets from northwestern North America tend
514 to produce R^2_c values above the 0.45-0.55 range, while this range is in the upper tail of
515 the R^2_c distribution in MPI-ESM-P (Figure S8). The subsets of predictors yielding the
516 highest R^2_c values among the considered random sets delineate the upper bound of this
517 reconstruction method by the inclusion of improved predictors. Accordingly, analogously
518 to Figure 7a, Figure 7b summarizes the skill metrics for the subset of pseudo-
519 reconstructions with R^2_c values in the upper quartile of the R^2_c distribution. BCC-CSM1-
520 1, CCSM4 and less so GISS-R24 and IPSL-CM5A-LR indicate upper potential for the
521 TT2010 approach, especially in terms of R^2_v (compare panels a and b in Figure 7). This is
522 not the case for FGOALS-gl, GISS-E2-R25 and MPI-ESM-P, whose best skill scores
523 indicate that pseudo-reconstructions from northwestern North American predictors are
524 unlikely capable of explaining substantially larger variance than obtained in the actual
525 TT2010 reconstruction. The simulations also disagree about whether an improved

526 selection of predictors would lead to more distinguishable reconstruction skills between
527 PNA and NPI (not shown).

528 The correlation patterns between the residuals of the PNA pseudo-reconstructions
529 illustrated in Figures 7a and 8 and North American winter temperatures (Figure 11)
530 indicate that, consistently among the simulations, an approach only using predictors from
531 northwestern North America lacks important information from the southwestern and
532 southeastern United States. Both regions correspond to characteristic regions for the PNA
533 signature on North American winter temperatures (Figure 2). The residual correlation
534 patterns and their robustness reflect structural deficiencies, and suggest possible changes
535 in the reconstruction design to improve PNA reconstructions. Inclusion of temperature
536 information from the southeastern United States would, for instance, reduce the risk of
537 erroneously interpreting periods of spatially uniform continental warming/cooling or
538 moistening/drying over North America as positive/negative PNA phases.

539 Accordingly, Figure 7c outlines the potential of the reconstruction method through an
540 improved selection of proxy locations and extended calibration period. In this case, the
541 predictor sets include temperature sampled from a box located over Florida instead of
542 precipitation sampled from the southern box over the western United States, so that the
543 model can capture information from the easternmost negative PNA center (Figures 1 and
544 2). The potential quality of the PNA pseudo-reconstructions obtained with this design is
545 greatly improved according to both considered skill metrics (compare panels b and c in
546 Figure 7). The quality of the pseudo-reconstructions still varies substantially through the
547 last millennium (not shown), but the risk of periods of unskillful reconstructions ($CE < 0$)
548 is much lower than for a design limited to northwestern North America. The pseudo-
549 reconstructions further display improvement in the negative bias and a substantially
550 better representation of low-frequency PNA variability (Figure S12). However, the
551 models disagree about which factor (*i.e.*, extended calibration period or inclusion of a
552 temperature predictor for the southeastern United States) more strongly contribute to the
553 improved results.

554 In summary, pseudo-proxy experiments appear to be instrumental in both the designing
555 and the assessment of future PNA reconstructions. Of course, the exemplary design
556 proposed here represents an ideal setting, and future applications of this tool for real-

557 world reconstructions would require the pseudo-proxy experiments to be designed based
558 on quality and type of actually available proxies.

559

560 **4. Discussion**

561 In order to understand the implications of our results for real-world proxy reconstructions
562 and for the interpretation of last-millennium climate simulations, our discussion
563 concentrates on three aspects: limitations of the reconstruction methods and of our
564 pseudo-reconstruction design in particular; weaknesses in the simulated representation of
565 the PNA, and of its teleconnections and variability; and issues related to (regional)
566 climate attribution before the observational period and uncertainties affecting the
567 simulation of the early-19th-century climate.

568 Our pseudo-proxy investigation reveals the inherent limitations of a PNA reconstruction
569 method solely relying on local geophysical predictors from northwestern North America.
570 Assumptions of linearity and stationarity between local hydro-climate variability and the
571 large-scale atmospheric circulation described by the PNA are further weaknesses of the
572 approach. In our linear definition, the PNA robustly dominates winter North American
573 climate variability (Figures 6), which is an encouraging premise for reconstruction
574 attempts. Nonetheless, the so-defined PNA index may not capture shifts in the location of
575 the mode's centers of action and in the associated teleconnections (Raible et al., 2014).
576 Furthermore, our pseudo-reconstructions can be affected by the non-stationarity of the
577 teleconnection pattern to North America of other modes of climate variability, like ENSO
578 (Coats et al., 2013). Pseudo-reconstructions suggest that margins exist to substantially
579 improve the quality of the reconstructed PNA based on a TT2010-like multi-linear
580 regression method, for instance if the multiple PNA-sensitive regions over North
581 America are more exhaustively represented in the predictors' set and if the calibration
582 period is extended. However, including temperature-sensitive predictors from the
583 southeastern North America and extending the calibration period to the full 20th century,
584 as in our pseudo-proxy experiment (Figure 7c), may be difficult due to the nature of real-
585 world climate proxies and limitation of observational data suitable for model calibration.
586 First, as noted above, the ensemble teleconnection patterns in Twentieth-Century-

587 Reanalysis data – the longest reanalysis product now available – are poorly constrained
588 during the first half of the 20th century over the Pacific (Raible et al., 2014). Then, the
589 Northern Hemisphere’s ring-width network shows that the proxy-responses to
590 atmospheric modes like the PNA are determined by a complex causal chain linking large-
591 scale circulation, local climate and seasonal tree growth (St. George, 2014). Accordingly,
592 relatively few chronologies, mostly from the Pacific Northwest and northern Rockies,
593 significantly respond to the winter PNA (St. George, 2014). More generally, real climate-
594 proxies can be critically affected by noise ([von Storch et al., 2009](#)), and may suffer from
595 non-stationary climate-proxy relationships that are neglected in our perfect-model
596 framework (*e.g.*, Evans et al., 2013; D’Arrigo et al 2008). There exist, however, long
597 winter precipitation-sensitive, and possibly also temperature-sensitive, proxies across the
598 southern United States (*e.g.*, Stahle et al., 1994; St. George, 2014; St. George and Ault,
599 2014), upon which future designs of PNA pseudo-reconstruction exercises could be
600 based. [As shown in supplementary Figure S13, the skills of an ensemble of TT2010-like
601 PNA pseudo-reconstructions progressively deteriorate for increasing levels of noise
602 artificially introduced in the predictors. Skills depend more on the level of noise rather
603 than on the type of noise, at least for low amounts of noise, in accordance with von
604 Storch et al. \(2009\). For a signal-to-noise ratio of 1 \(Figure S13c,f\) explained variances
605 for the validation period never reach 0.5, and red noise generally produces unskillful
606 reconstructions.](#) So, our pseudo-proxy investigation is only meant as an idealized
607 example demonstrating the potential margins of improvement offered by the
608 reconstruction method. Its application to a real-world PNA reconstruction requires
609 scrutiny of available data, which we defer to a follow-up dedicated study.

610 Poor modeling of the PNA-related dynamics is a straightforward explanation of the early-
611 19th century discrepancy between the reconstruction and the simulations. Furthermore,
612 the realism of our PNA pseudo-reconstructions relies on the realism of simulated
613 patterns, variability and teleconnections of the PNA as well as of other hemispheric
614 modes imprinting on the North American climate. Accurate representation of observed
615 dominant modes of climate variability and of their teleconnections still represents a
616 challenge for coupled climate simulations (*e.g.*, about ENSO see: Guilyardi et al., 2012;

617 Zou et al., 2014). Unrealistic simulated representation of large-scale atmospheric
618 circulation modes can arise due to biased ocean-atmosphere coupling over remote
619 regions: Coupled climate models are still affected by considerable biases in regional
620 SSTs and sea ice - especially in the North Atlantic Ocean - that are associated, in the
621 Northern Hemisphere, to cold biases resembling the Northern Hemisphere's annular
622 mode (Wang et al., 2014). This suggests that good model performance in simulating
623 regional processes may be overridden by the effect of remote biases.

624 Our definition of the PNA index does not account for possible displacements of its
625 centers of actions in simulated patterns compared to reanalyses. An alternative definition
626 based on empirical orthogonal functions (EOF) results in PNA indices that share between
627 half (MIROC-ESM) and almost the whole (CCSM4) total variance with the pointwise-
628 based PNA indices over the observational period (see supplementary Table S1). Spatial
629 differences between simulated EOF-based and pointwise-based patterns also vary
630 considerably across the ensemble (Table S1). It is not yet clear whether and how these
631 uncertainties related to the index definition affect the details of the pseudo-
632 reconstructions. The validity of our general conclusions clearly stands for the sub-
633 ensemble including only models with the most consistent PNA indices across the two
634 definitions (CCSM4, IPSL-CM5A-LR, MPI-ESM-P).

Deleted: ¶

635 The marked inter-model differences in the PNA-precipitation correlation patterns over
636 North America and their general disagreement with the observed pattern (Figure 3)
637 highlight the large uncertainties in the connection between large-scale circulation and
638 local hydro-climates that still affect state-of-the-art coupled climate simulations. In this
639 regard, topography largely determines the wave-like structure of the PNA and its surface
640 signature. Its dominant role was already highlighted by TT2010 in describing the
641 characteristics of their two precipitation-sensitive tree-ring series from Montana and
642 Wyoming. Poor model topography likely leads to biases in representing the PNA pattern
643 and more visibly its climate fingerprints. This was exemplified here by the stark contrast
644 between the low-resolution model FGOALS-g1 and the high-resolution model CCSM4
645 (compare panels c and d in Figures 1-3). With few exceptions, topography in the
646 employed models misses critical plateau elevations that are crucial for the onset and

Deleted: A p

647 sustenance of snow/ice-related feedbacks (Berdahl and Robock, 2013). These could be
648 relevant for the reinforcement/dampening of the Canadian High during the development
649 phase of a positive/negative PNA (Ge and Gong, 2009). Accordingly, these latter model
650 deficiencies can partly explain why inclusion of precipitation over the Rockies as a
651 predictor degrades the skills of our pseudo-reconstructions and yields much weaker skills
652 than the actual TT2010 reconstruction (as discussed in section 2.4).

Deleted:

653 A possible solution to the discrepancy between the reconstruction and the simulations is
654 to attribute the reconstructed early-19th-century positive PNA phase to internal
655 variability. Supporting this hypothesis, interdecadal persistent positive PNA phases
656 emerge in all simulations throughout the last millennium without consistent timing
657 (Figure 4a). However, simulated events are generally weaker than the reconstructed event
658 and the number of those longer than 20 years is exiguous (see supplementary Figure
659 S14). Therefore, notwithstanding the caveats described above about the realism of
660 simulated PNA dynamics and variability, the reconstructed early-19th-century positive
661 PNA phase is compatible with an exceptional event of internal climate variability. A
662 similar interpretation has been recently proposed, with the support of climate simulations,
663 for reconstructed multidecadal droughts in the southwestern North America during the
664 last millennium (Coats et al., 2015). Further supporting this hypothesis, the simulations
665 ensemble does not point to coherent positive PNA anomalies during other periods of the
666 last millennium with concomitant strong volcanic forcing and weak solar forcing, e.g.,
667 the mid 15th and the late 17th centuries (Figure 4a).

Deleted: ¶

Formatted: Superscript

Formatted: Superscript

668 Under the alternative hypothesis that the reconstructed early-19th-century positive PNA
669 phase is externally driven, the discrepancy between the reconstruction and the
670 simulations can be explained by common model deficiencies in the simulated dynamical
671 response to natural forcing and/or by uncertainty in the (reconstructed) imposed external
672 forcing. Supporting this hypothesis, state-of-the-art coupled climate models still suffer
673 from a deficient representation of stratospheric and coupled stratosphere-troposphere
674 dynamics (Kodera et al., 1996; Woollings et al., 2010), which affect the simulated
675 response to volcanic (Driscoll et al., 2012; Charlton-Perez et al., 2013; Muthers et al.
676 2014) and solar (Gray et al., 2010; Anet et al., 2014) forcing. Furthermore, inter-model

Deleted: Otherwise, solving the discrepancy becomes an issue of attribution.

Deleted: e first

677 disagreement about post-eruption oceanic evolutions (*e.g.*, Ding et al., 2014) shows that
678 large uncertainties still exist about decadal-scale climate variability during periods of
679 strong volcanic forcing and the role of the ocean in determining the surface-air
680 temperature response (Canty et al., 2013). Sensitivity simulations performed with a
681 chemistry–climate model demonstrate the importance of the Dalton Minimum of solar
682 activity for the persistence of the hemispheric cold temperature anomalies of the early
683 19th century (Anet et al., 2014). Yet, the cold winter temperature anomalies depicted by
684 these simulations over Alaska during the period 1805-1825 do not match with the imprint
685 of a positive PNA. Single-model ensemble climate simulations have shown that the 1815
686 Tambora eruption produces robust large-scale atmospheric circulation anomalies, roughly
687 corresponding to a positive PNA phase, only in the absence of additional external
688 disturbances, whereas under full-forcing conditions such positive PNA-like features
689 become hardly distinguishable (Zanchettin et al., 2013a). The same simulation-ensembles
690 have further demonstrated that internal climate variability can be a source of uncertainty
691 for the simulated early-19th-century decadal climate evolution as important as the
692 (reconstructed) imposed forcing (Zanchettin et al., 2013a). Moreover, although climate
693 simulations depict an interannual to decadal PNA/NPI response to strong tropical
694 volcanic eruptions (Zanchettin et al., 2012; Wang et al., 2012), responses on longer time
695 scales may be damped by the resilience of the interdecadal component of the Pacific
696 Decadal Oscillation to natural external forcing (Zanchettin et al., 2013b).

697 Uncertainty in the external forcing factors acting on the early-19th-century climate further
698 complicates the attribution of reconstructed and simulated variability. For instance,
699 reconstructed variations in total solar irradiance are affected by considerable uncertainties
700 (*e.g.*, Schmidt et al., 2011; Shapiro et al., 2011) as well as deficiencies in accounting for
701 the spectrum variations for solar forcing and ozone response (Gray et al. 2010). Debate is
702 ongoing about how changes in total solar irradiance affect the tropical oceans, with
703 different observations and different simulations disagreeing about whether warming
704 rather than cooling of the upper tropical Pacific is expected under enhanced solar activity
705 (Misios and Schmidt, 2012). Moreover, the radiative impact of tropical volcanic
706 eruptions is sensitive to the season of the eruption (Toohey et al., 2011; Froelicher et al.,

707 2013), and the season of the 1809 tropical eruption is still insufficiently constrained
708 (Cole-Dai et al., 2009).

709 **5. Conclusions**

710 Our results depict a discrepancy between reconstructed and simulated PNA behavior
711 during the early 19th century, an exceptionally cold period [in the Northern Hemisphere](#)
712 characterized by concomitant weak solar and strong volcanic forcing. According to our
713 pseudo-proxy investigation, reconstructions based on northwestern North American
714 geophysical predictors are potentially skillful in terms of two different metrics
715 (coefficient of determination and coefficient of error). Such an approach following Trouet
716 and Taylor (2010) is also likely capable of capturing strong interdecadal positive PNA
717 phases, like the one reconstructed for the early 19th century. However, a number of
718 sources of uncertainty and potential deficiencies are still present especially at
719 multidecadal and centennial timescales. Furthermore, pseudo-reconstructions based
720 solely on predictors from northwestern North America often cannot distinguish between
721 the PNA and the North Pacific Index describing the strength of the Aleutian Low.

722 The *PMIP3-past1000* and *historical* simulations provide an overall satisfactory
723 representation of the observed PNA spatial pattern and of its imprint on the North
724 American climate. Simulated pre-industrial PNA evolutions show a predominance of
725 internal variability over forced signals, which could be used as an argument to explain
726 why simulations do not robustly exhibit the reconstructed positive PNA phase in the early
727 19th century. Shifting focus to attribution of the reconstructed anomaly requires
728 confidence that simulations do not suffer from common deficiencies in the response to
729 natural forcing, in the applied reconstructed forcing and/or in the internally-generated
730 climate variability. We need therefore to better understand the relative role of externally-
731 forced and internal climate variability during the pre-industrial period.

732 A refined topography associated with high horizontal model resolution appears to be
733 essential for models to realistically capture the connection between the large-scale
734 circulation and the local climatic/environmental conditions upon which a reliable PNA

735 reconstruction depends. However, our pseudo-reconstructions also indicate that there is
736 margin to substantially improve the available PNA reconstruction, in particular through a
737 more exhaustive representation of the multiple PNA-sensitive regions over North
738 America in the predictors' set. These results call for strengthened cooperation between
739 the climate-proxy and climate modeling communities in order to improve our knowledge
740 about the early-19th-century PNA and to solve the related reconstruction-simulations
741 discrepancy.

742

743 **Acknowledgments**

744 This study stems from discussion during the PAGES2k/PMIP "Workshop on integrated
745 analyses of reconstructions and multi-model simulations for the past two millennia"
746 (<http://www.palma-ucm.es/members/workshop/Home.html>) in November 2013, funded
747 by PAGES, FECYT-MINECO and IGEO. [Comments from two anonymous reviewers](#)
748 [helped improve the clarity of the manuscript.](#) Thomas Kleinen provided useful comments
749 on an earlier version of the draft. D. Zanchettin was supported by the BMBF (research
750 program "MiKlip", FKZ:01LP1158A). F. Lehner and C. C. Raible are supported by the
751 Swiss National Science Foundation. This work contributes to the MPI-M Integrated
752 Project Millennium and CliSAP. We acknowledge the World Climate Research
753 Programme's Working Group on Coupled Modelling, which is responsible for CMIP,
754 and we thank the climate-modelling groups for producing and making available their
755 model output.

756

757 **References**

- 758 Ammann, C. M., Joos, F., Schimel, D. S., Otto-Bliesner, B. L. and Tomas, R. A. (2007) Solar influence on
759 climate during the past millennium: results from transient simulations with the NCAR Climate
760 System Model. *Proc. Natl. Acad. Sci. U. S. A.*, **104**, 3713–3718.
- 761 Anet, J. G., S. Muthers, E. V. Rozanov, C. C. Raible, A. Stenke, A. I. Shapiro, S. Brönnimann, F. Arfeuille,
762 Y. Brugnara, J. Beer, F. Steinhilber, W. Schmutz, and T. Peter (2014) Impact of solar versus
763 volcanic activity variations on tropospheric temperatures and precipitation during the Dalton
764 Minimum. *Clim. Past*, 10, 921–938, doi:10.5194/cp-10-921-2014.

- 765 Barnston, A. G., and R. E. Livezey, 1987: Classification, seasonality and persistence of low-frequency
766 atmospheric circulation patterns. *Mon. Wea. Rev.*, **115**, 1083–1126.
- 767 Baxter, S., and S. Nigam (2013) A subseasonal teleconnection analysis: PNA development and its
768 relationship to the NAO. *J. Climate*, **26**, 6733–674.
- 769 Berdahl, M., and A. Robock (2013), Northern Hemispheric cryosphere response to volcanic eruptions in
770 the Paleoclimate Modeling Intercomparison Project 3 last millennium simulations, *J. Geophys.*
771 *Res. Atmos.*, **118**, 12,359–12,370, doi:10.1002/2013JD019914.
- 772 Bothe, O., Jungclaus, J. H., and Zanchettin, D. (2013) Consistency of the multi-model CMIP5/PMIP3-
773 past1000 ensemble. *Clim. Past*, **9**, 2471–2487, doi:10.5194/cp-9-2471-2013.
- 774 Braconnot, P., S. P. Harrison, M. Kageyama, P. J. Bartlein, V. Masson-Delmotte, A. Abe-Ouchi, B. Otto-
775 Bliesner, and Y. Zhao (2012) Evaluation of climate models using palaeoclimatic data, *Nature*
776 *Clim. Ch.*, **2**, 417–424, doi:10.1038/nclimate1456.
- 777 Canty, T., N. R. Mascioli, M. D. Smarte, and R. J. Salawitch (2013) An empirical model of global climate
778 – Part 1: A critical evaluation of volcanic cooling. *Atm. Chem. Phys.*, **13**, 3997–4031,
779 doi:10.5194/acp-13-3997-2013.
- 780 Charlton-Perez, A. J., Baldwin, M. P., Birner, T., Black, R. X., Butler, A. H., Calvo, N., Davis, N. A.,
781 Gerber, E. P., Gillett, N., Hardiman, S., Kim, J., Krüger, K., Lee, Y.-Y., Manzini, E., Mc-Daniel,
782 B. A., Polvani, L., Reichler, T., Shaw, T. A., Sigmond, M., Son, S.-W., Toohey, M., Wilcox, L.,
783 Yoden, S., Christiansen, B., Lott, F., Shindell, D., Yukimoto, S., and Watanabe, S.: On the lack of
784 stratospheric dynamical variability in low-top versions of the CMIP5 models, *J. Geophys. Res.*,
785 **118**, 2494–2505, doi:10.1002/jgrd.50125, 2013.
- 786 [Coats, S., J. E. Smerdon, B. I. Cook, and R. Seager \(2013\) Stationarity of the tropical pacific teleconnection
787 to North America in CMIP5/PMIP3 model simulations. *Geophys. Res. Lett.*, **40**\(18\), 4927–4932,
788 doi:10.1002/grl.50938](#)
- 789 [Coats, S., J. E. Smerdon, B. I. Cook, and R. Seager \(2015\) Are Simulated Megadroughts in the North
790 American Southwest Forced?. *J. Climate*, **28**, 124–142. doi:http://dx.doi.org/10.1175/JCLI-D-14-
791 00071.1](#)
- 792 Cole-Dai, J., D. Ferris, A. Lanciki, J. Savarino, M. Baroni, and M. H. Thiemens (2009), Cold decade (AD
793 1810–1819) caused by Tambora (1815) and another (1809) stratospheric volcanic eruption,
794 *Geophys. Res. Lett.*, **36**, L22703, doi:10.1029/2009GL040882.
- 795 Compo, G. P., Whitaker, J. S., Sardeshmukh, P. D., Matsui, N., Allan, R. J., Yin, X., Gleason Jr., B. E.,
796 Vose, R. S., Rutledge, G., Bessemoulin, P., Broennimann, S., Brunet, M., Crouthamel, R. I.,
797 Grant, A. N., Groisman, P. Y., Jones, P. D., Kruk, M. C., Kruger, A. C., Marshall, G. J., Maugeri,
798 M., Mok, H. Y., Nordli, O., Ross, T. F., Trigo, R. M., Wang, X. L., Woodruff, S. D., and Worley,
799 S. J. (2011) The Twentieth Century Reanalysis Project, *Q. J. Roy. Meteorol. Soc.*, **137**, 1–28.
- 800 Cook, E. R., K. R. Briffa, and P. D. Jones (1994) Spatial regression methods in dendroclimatology – a
801 review and comparison of 2 techniques. *Int. J. Climatol.*, **14**, 379–402.
- 802 Crowley, T. J. (2000) Causes of climate change over the past 1000 years, *Science*, **289**, 270–277.
- 803 Crowley, T. J., Zielinski, G., Vinther, B., Udisti, R., Kreutz, K., Cole-Dai, J., and Castellano, E. (2008)
804 Volcanism and the little ice age, *Pages News*, **16**, 22–23.

- 805 D'Arrigo, R., R. Wilson, B. Liepert, and P. Cherubini (2008) On the 'Divergence Problem' in Northern
806 Forests: A review of the tree-ring evidence and possible causes. *Glob. Plan. Ch.*, **60**, 289-305
- 807 Ding, Y., J. A. Carton, G. A. Chepurin, G. Stenchikov, A. Robock, L. T. Sentman, and J. P. Krasting
808 (2014) Ocean response to volcanic eruptions in Coupled Model Intercomparison Project 5
809 (CMIP5) simulations. *J. Geophys. Res.*, in press, doi:10.1002/2013JC009780.
- 810 Driscoll, S., A. Bozzo, L. J. Gray, A. Robock, and G. Stenchikov (2012) Coupled Model Intercomparison
811 Project 5 (CMIP5) simulations of climate following volcanic eruptions, *J. Geophys. Res.*, **117**,
812 D17105, doi:10.1029/2012JD017607.
- 813 Dufresne, J.-L., Foujols, M.-A., Denvil, S., Caubel, A., Marti, O., Aumont, O., Balkanski, Y., Bekki, S.,
814 Bellenger, H., Benshila, R., Bony, S., Bopp, L., Braconnot, P., Brockmann, P., Cadule, P., Cheruy,
815 F., Codron, F., Cozic, A., Cugnet, D., de Noblet, N., Duvel, J.-P., Ethé, C., Fairhead, L., Fichet,
816 T., Flavoni, S., Friedlingstein, P., Grandpeix, J.-Y., Guez, L., Guilyardi, E., Hauglustaine, D.,
817 Hourdin, F., Idelkadi, A., Ghattas, J., Joussaume, S., Kageyama, M., Krinner, G., Labetoulle, S.,
818 Lahellec, A., Lefebvre, M.-P., Lefevre, F., Levy, C., Li, Z. X., Lloyd, J., Lott, F., Madec, G.,
819 Mancip, M., Marchand, M., Masson, S., Meurdesoif, Y., Mignot, J., Musat, I., Parouty, S.,
820 Polcher, J., Rio, C., Schulz, M., Swingedouw, D., Szopa, S., Talandier, C., Terray, P., and Viovy,
821 N. (2013) Climate change projections using the IPSL-CM5 Earth System Model: from CMIP3 to
822 CMIP5. *Clim. Dyn.*, **40**, 2123-2165.
- 823 Evans, M.N., S.E. Tolwinski-Ward, D.M. Thompson, and K.J. Anchukaitis (2013) Applications of proxy
824 system modeling in high resolution paleoclimatology. *Quat. Sc. Rev.*, **76**, 16-28,
825 doi:10.1016/j.quascirev.2013.05.024.
- 826 Froelicher, T. L., F. Joos, C. C. Raible, J. L. Sarmiento (2013) Atmospheric CO2 response to volcanic
827 eruptions: the role of ENSO, season, and variability. *Global Biogeochemical Cycles*, **27**, 239-251.
- 828 Gao, C., A. Robock, and C. Ammann (2008) Volcanic forcing of climate over the past 1500 years: an
829 improved ice core-based index for climate models, *J. Geophys. Res.-Atmos.*, **113**, D23111,
830 doi:10.1029/2008JD010239.
- 831 Ge, Y., and G. Gong (2009) North American snow depth and climate teleconnection patterns. *J. Clim.*, **22**,
832 217-233, doi:10.1175/2008JCLI2124.1.
- 833
834 Gong, D.-Y., R. Mao, P.-J. Shi, Y.-D. Fan (2007) Correlation between east Asian dust storm frequency and
835 PNA. *Gephys. Res. Lett.*, **34**, L14710, doi:10.1029/2007GL029944.
- 836 Gray, L. J., Beer, J., Geller, M., Haigh, J. D., Lockwood, M., Matthes, K., Cubasch, U., Fleitmann, D.,
837 Harrison, G., Hood, L., Luterbacher, J., Meehl, G. A., Shindell, D., van Geel, B., and White, W.
838 (2010) Solar influence on climate, *Rev. Geophys.*, **48**, RG4001, doi:10.1029/2009RG000282.
- 839 Guilyardi, E., H. Bellenger, M. Collins, S. Ferrett, W. Cai, and A. Wittenberg (2012) First look at ENSO in
840 CMIP5. *CLIVAR Exchanges No. 58*, Vol. 17, No.1.
- 841 Horel, J.D., and Wallace J.M. (1981) Planetary-scale atmospheric phenomena associated with the southern
842 oscillation. *Mon. Weath. Rev.*, **109**, 813-829.
- 843 Hubeny, J. B., J. W. King, M. Reddin (2010) Northeast US precipitation variability and North American
844 climate teleconnections interpreted from late Holocene varved sediments. *Proc. Nat. Ac. Sc.*, **108**,
845 17895-17900, doi:10.1073/pnas.1019301108.

- 846 Jones, P., and Mann, M. (2004) Climate over past millennia, *Rev. Geophys.*, **42**, RG2002,
847 doi:10.1029/2003RG000143.
- 848 Jungclauss, J. H., K. Lohmann, and D. Zanchettin (2014) Enhanced 20th century heat transfer to the Arctic
849 simulated in the context of climate variations over the last millennium. *Clim. Past Discuss.* **10**,
850 2895-2924, doi:10.5194/cpd-10-2895-2014
- 851 Kalnay, E., M. Kanamitsu, R. Kistler, W. Collins, D. Deaven, L. Gandin, M. Iredell, S. Saha, G. White, J.
852 Woollen, Y. Zhu, A. Leetmaa, R. Reynolds, M. Chelliah, W. Ebisuzaki, W. Higgins, J. Janowiak,
853 K. C. Mo, C. Ropelewski, J. Wang, Roy Jenne, and D. Joseph (1996) The NCEP/NCAR 40-Year
854 Reanalysis Project. *Bull. Amer. Meteor. Soc.*, **77**, 437–471.
- 855 Kistler, R., W. Collins, S. Saha, G. White, J. Woollen, E. Kalnay, M. Chelliah, W. Ebisuzaki, M.
856 Kanamitsu, V. Kousky, H. van den Dool, R. Jenne, and M. Fiorino, (2001) The NCEP–NCAR 50–
857 Year Reanalysis: Monthly means CD–ROM and Documentation. *Bull. Amer. Meteor. Soc.*, **82**,
858 247–267.
- 860 Kodera, K., Chiba, M., Koide, H., Kitoh, A., and Nikaidou, Y. (1996) Interannual variability of the winter
861 stratosphere and troposphere in the Northern Hemisphere, *J. Meteorol. Soc. Jpn.*, **74**, 365–382.
- 862 Landrum, L., Otto-Bliessner, B. L., Wahl, E. R., Conley, A., Lawrence, P. J., Rosenbloom, N., and Teng, H.
863 (2011) Last millennium climate and its variability in CCSM4, *J. Climate*, **26**, 1085–1111,
864 doi:10.1175/jcli-d-11-00326.1.
- 865 Lehner, F., C. C. Raible, and T. F. Stocker (2012) Testing the robustness of a precipitation proxy-based
866 North Atlantic Oscillation reconstruction. *Quat. Sc. Rev.* **45**, 85-94,
867 doi:10.1016/j.quascirev.2012.04.025
- 868 ~~Li, J., Xie, S.-P., Cook, E. R., Morales, M. S., Christie, D. A., Johnson, N. C., Chen, F., D'Arrigo, R.,
869 Fowler, A. M., Gou, X., and Fang, K. (2013) El Niño modulations over the past seven centuries,
870 *Nature Cl. Ch.*, **3**, 822–826, doi:10.1038/NCLIMATE1936~~
- 871 Macias-Fauria, M., A. Grinsted, S. Helama, and J. Holopainen (2012) Persistence matters: Estimation of the
872 statistical significance of paleoclimatic reconstruction statistics from autocorrelated time series.
873 *Dendrochronol.*, **30**, 179-187.
- 874 Mann, M. E., Zhang, Z., Rutherford, S., Bradley, R. S., Hughes, M. K., Shindell, D., Ammann, C.,
875 Faluvegi, G., and Ni, F. (2009) Global signatures and dynamical origins of the Little Ice Age and
876 Medieval Climate Anomaly, *Science*, **326**, 1256–1260, doi:10.1126/science.1177303.
- 877 Misios, S., H. Schmidt (2012) Mechanisms Involved in the Amplification of the 11-yr solar cycle signal in
878 the tropical Pacific ocean. *J. Climate*, **25**, 5102–5118.
- 879 Moore, G. W. K., I. A. Renfrew, and R. S. Pickart (2013) Multidecadal mobility of the North Atlantic
880 Oscillation, *J. Climate*, **26**, 2453–2466.
- 881 Muthers, S., J. G. Anet, E. Rozanov, C. C. Raible, T. Peter, A. Stenke, A. Shapiro, J. Beer, F. Steinhilber,
882 S. Broennimann, F. Arfeuille, Y. Brugnara, and W. Schmutz (2014) Sensitivity of the winter
883 warming pattern following tropical volcanic eruptions to the background ozone climatology, *J.*
884 *Geophys. Res.*, **119**, 1340-1355. DOI:10.1002/2013JD020138.

Formatted: English (U.S.)

Formatted: English (U.S.)

Deleted: .

- 885 Notaro, M., W.-C. Wang, W. Gong (2006) Model and Observational Analysis of the Northeast U.S.
886 Regional Climate and Its Relationship to the PNA and NAO Patterns during Early Winter.
887 *Monthly Weather Review* **134**, 3479-3505.
- 888 Pinto, J. G., Reyers, M., Ulbrich, U. (2011) The variable link between PNA and NAO in observations and
889 in multi-century CGCM simulations. *Clim. Dyn.* **36**, 337-354, doi:10.1007/s00382-010-0770-x.
- 890 Raible, C. C., U. Luksch, K. Fraedrich, and R. Voss (2001) North Atlantic decadal regimes in a coupled
891 GCM simulation, *Clim. Dyn.*, **18**, 321-330.
- 892 Raible, C. C., Casty, C., Luterbacher, J., Pauling, A., Esper, J., Frank, D. C., Büntgens, U., Roesch, A. C.,
893 Wild, M., Tschuck, P., Vidale, P.-L., Schär, C., and Wanner, H. (2006) Climate variability –
894 observations, reconstructions and model simulations, *Climatic Change*, **79**, 9–29.
- 895 Raible, C. C., F. Lehner, J. F. González-Rouco, and L. Fernández-Donado (2014) Changing correlation
896 structures of the Northern Hemisphere atmospheric circulation from 1000 to 2100 AD. *Clim. Past*,
897 **10**, 537-550, doi:10.5194/cp-10-537-2014.
- 898 Shapiro, A. I., W. Schmutz, E. Rozanov, M. Schoell, M. Haberleiter, A. V. Shapiro and S. Nyeki (2011) A
899 new approach to the long-term reconstruction of the solar irradiance leads to large historical solar
900 forcing. *Astr. & Astrophys.*, **529**, A67, doi: <http://dx.doi.org/10.1051/0004-6361/201016173>.
- 901 Schmidt, G. A., Annan, J. D., Bartlein, P. J., Cook, B. I., Guilyardi, E., Hargreaves, J. C., Harrison, S. P.,
902 Kageyama, M., LeGrande, A. N., Konecky, B., Lovejoy, S., Mann, M. E., Masson-Delmotte, V.,
903 Risi, C., Thompson, D., Timmermann, A., Tremblay, L.-B., and Yiou, P.: Using paleo-climate
904 comparisons to constrain future projections in CMIP5, *Clim. Past Discuss.*, **9**, 775–835,
905 doi:10.5194/cpd-9-775-2013, 2013.
- 906 Smerdon, J. E. (2012) Climate models as a test bed for climate reconstruction methods: pseudoproxy
907 experiments. *WIREs Clim Change*, **3**, 63–77, doi: 10.1002/wcc.149.
- 908 Stahle, D. W., and M. K. Cleaveland (1994) Tree-ring reconstructed rainfall over the southeastern USA
909 during the medieval warm period and the little ice age. *Clim. Change*, **26**, 199-212.
- 910 St. George, S. (2014) An overview of tree-ring width records across the Northern Hemisphere. *Quat. Sc.*
911 *Rev.*, **95**, 132-150, doi:10.1016/j.quascirev.2014.04.029.
- 912 St. George, S., and T. R. Ault (2014) The imprint of climate within Northern Hemisphere trees. *Quat. Sc.*
913 *Rev.*, **89**, 1-4, doi:10.1016/j.quascirev.2014.01.007.
- 914 Starheim, C.C.A., Smith, D.J., Prowse, T.D., 2013, Dendrohydroclimate reconstructions of July-August
915 runoff for two nival-regime rivers in west central British Columbia. *Hydrol. Proc.*, **27**, 405-420.
- 916 Stephenson, D. B., V. Pavan, M. Collins, M. M. Junge, and R. Quadrelli (2006) North Atlantic Oscillation
917 response to transient greenhouse gas forcing and the impact on European winter climate: a CMIP2
918 multi-model assessment. *Clim. Dyn.*, **27**, 401–420, doi:10.1007/s00382-006-0140-x.
- 919 Toohey, M., Krüger, K., Niemeier, U. and Timmreck, C. (2011) The influence of eruption season on the
920 global aerosol evolution and radiative impact of tropical volcanic eruptions *Atmosph. Chem.*
921 *Phys.*, **11**, 12351-12367, doi:10.5194/acp-11-12351-2011.
- 922 Trenberth, K. E., and J. W. Hurrell (1994) Decadal atmosphere-ocean variations in the Pacific. *Clim. Dyn.*,
923 **9**, 303-319.

- 924 Trouet, V., and A. H. Taylor (2010) Multi-century variability in the Pacific North American circulation
925 pattern reconstructed from tree rings. *Clim. Dyn.*, **35**, 953–963, doi:10.1007/s00382-009-0605-9.
- 926 Vieira, L. E. A., Solanki, S. K., Krivova, N. A., and Usoskin, I. (2011) Evolution of the solar irradiance
927 during the Holocene, *Astr. Astrophys.*, **531**, A6, doi:10.1051/0004-6361/201015843.
- 928 [von Storch, H., E. Zorita, F. Gonzalez-Rouco \(2009\) Assessment of three temperature reconstruction
929 methods in the virtual reality of a climate simulation. *Int. J. Earth. Sci. \(Geol Rundsch\)* 98:67–82,
930 doi:10.1007/s00531-008-0349-5](#)
- 931 Wahl, E. R., and J. E. Smerdon (2012) Comparative performance of paleoclimate field and index
932 reconstructions derived from climate proxies and noise-only predictors, *Geophys. Res. Lett.*, **39**,
933 L06703, doi:10.1029/2012GL051086.
- 934 Wahl, E. R., Diaz, H. F., Smerdon, J. E., and C. M. Ammann (2014) Late winter temperature response to
935 large tropical volcanic eruptions in temperate Western North America: Relationship to ENSO
936 phases, *Glob. Plan. Ch.*, online first, doi:10.1016/j.gloplacha.2014.08.005.
- 937 Wallace, J. M., and D. S. Gutzler (1981) Teleconnections in the Geopotential Height Field during the
938 Northern Hemisphere Winter. *Mon. Wea. Rev.*, **109**, 784–812, doi:http://dx.doi.org/10.1175/1520-
939 0493(1981)109<0784:TITGHF>2.0.CO;2.
- 940 Wang, C., L. Zhang, S.-K. Lee, L. Wu, and C. R. Mechoso (2014) A global perspective on CMIP5 climate
941 model biases. *Nature Clim. Ch.*, **4**, 201–205, doi:10.1038/nclimate2118.
- 942 Wang, T., O. H. Otterå, Y. Gao, and H. Wang (2012), The response of the North Pacific Decadal
943 Variability to strong tropical volcanic eruptions. *Clim. Dyn.*, **39**, 2917–2936, doi:10.1007/s00382-
944 012-1373-5.
- 945 Woollings, T., Charlton-Perez, A., Ineson, S., Woollings, T., Charlton-Perez, A., Ineson, S., Marshall, A.
946 G., and Masato, G. (2010) Associations between stratospheric variability and tropospheric
947 blocking, *J. Geophys. Res.*, **115**, D06108, doi:10.1029/2009JD012742.
- 948 Younas, W., and Y. Tang. (2013) PNA predictability at various time scales. *J. Climate* **26**, 9090–9114.
- 949 Yu, B., F. W. Zwiers. (2007) The impact of combined ENSO and PDO on the PNA climate: A 1,000-year
950 climate modeling study. *Clim. Dyn.*, **29**, 837–851.
- 951 Yu, B., A. Shabbar, F. W. Zwiers. (2007) The Enhanced PNA-Like climate response to Pacific interannual
952 and decadal variability. *J. Climate* **20**, 5285–5300.
- 953 Zanchettin, D., C. Timmreck, H.-F. Graf, A. Rubino, S. Lorenz, K. Lohmann, K. Krueger, and J. H.
954 Jungclaus (2012) Bi-decadal variability excited in the coupled ocean–atmosphere system by strong
955 tropical volcanic eruptions. *Clim. Dyn.*, **39**, 419–444, doi:10.1007/s00382-011-1167-1.
- 956 Zanchettin, D., O. Bothe, H. F. Graf, S. J. Lorenz, J. Luterbacher, C. Timmreck and J. H. Jungclaus (2013a)
957 Background conditions influence the decadal climate response to strong volcanic eruptions, *J.*
958 *Geophys. Res. Atmos.*, **118**, doi:10.1002/jgrd.50229.
- 959 Zanchettin, D., Rubino, A., Matei, D., and J.H. Jungclaus. (2013b) Multidecadal-to-centennial SST
960 variability in the MPI-ESM simulation ensemble for the last millennium. *Clim. Dyn.*, **40**, 1301-
961 1318, doi:10.1007/s00382-012-1361-9

Deleted: .

962 [Zanchettin, D., O. Bothe, C. Timmreck, J. Bader, A. Beitsch, H.-F. Graf, D. Notz and J. H. Jungclaus](#)
 963 [\(2014\) Inter-hemispheric asymmetry in the sea-ice response to volcanic forcing simulated by MPI-](#)
 964 [ESM \(COSMOS-Mill\). Earth Syst. Dynam., 5, 223–242, doi:10.5194/esd-5-223-2014](#)

965 Zhou, T., Li, B., Man, W., Zhang, L., and Zhang, J. (2011) A comparison of the Medieval Warm Period,
 966 Little Ice Age and 20th century warming simulated by the FGOALS climate system model,
 967 Chinese Sci. Bull., **56**, 3028–3041, doi:10.1007/s11434-011-4641-6.

968 Zou, Y., J.-Y. Yu, T. Lee, M.-M. Lu, and S. T. Kim (2014), CMIP5 model simulations of the impacts of the
 969 two types of El Niño on the U.S. winter temperature, J. Geophys. Res. Atmos., **119**,
 970 doi:10.1002/2013JD021064.

971

972

973 **TABLES**

Model/simulation	Components and resolutions	Natural forcing	Time intervals	References
BCC-CSM1-1 (rli1p1)		S: Vieira, V: Gao	P (850-1850) H (1851-2012)	-
CCSM4 (rli1p1)	CAM4 (1.25°x0.9°L26)/Parallel Ocean Model 2 (1°L60)	S: Vieira, V: Gao	P (850-1850) H (1851-2005)	Landrum et al. (2011)
FGOALS-gl (rli1p1)		S/V: Crowley (2000), Jones and Mann	P (1000-1999)	Zhou et al. (2011)
GISS-E2-R (rli1p124)	ModelE(2°x 2.5°L40)/Russell (1°x 1.25°L32)	S: Vieira, V: Crowley (2008)	P (850-1850) H (1851-2005)	-
GISS-E2-R (rli1p125)	ModelE(2°x 2.5°L40)/Russell (1°x 1.25°L32)	S: Vieira, V: Gao	P (850-1850) H (1851-2005)	http://data.giss.nasa.gov/mode/IE/ar5/
IPSL-CM5A-LR (rli1p1)	LMDZ5A (1.875°x3.75° L39)/NEMO (2° , with refinement at the equator of 0.5°, L31)	S: Vieira, V: Ammann et al. (2007)	P (850-1850) H (1851-2005)	Dufresne et al. (2013)
MIROC-ESM (rli1p1)	-	-	P (850-1850) H (1851-2005)	-
MPI-ESM-P (rli1p1)	ECHAM6 (T63L47)/MPIOM(GR15 L40)	S: Vieira, V: Crowley (2008)	P (850-1850) H (1851-2005)	Jungclaus et al. (2014)

974 Table 1 – Simulations considered in this study. Columns, from left: model and, in
 975 brackets, simulation; atmospheric and oceanic components (with resolution in brackets);
 976 applied external forcings for solar (S) and volcanic (V); considered periods of the
 977 past1000 (P) and historical (H) integrations; references/sources of information. Names of
 978 models and simulations follow the acronyms adopted in the CMIP5 repository. Full

979 references for the applied solar and volcanic forcing are: Vieira et al. (2011), Gao et al.
980 (2008), Crowley (2000), Jones and Mann (2004) and Crowley et al. (2008).

981

982

983 Figure captions

984 Figure 1 – Observed and simulated correlation maps between the winter PNA index and
985 winter Z500 time series for the period 1950-2005. Dots mark grid points where the
986 correlation is not significant at 95% confidence accounting for autocorrelation. The green
987 contours mark the boxes used for the calculation of the PNA index. In panels b-i, the
988 numbers reported in the title are the spatial correlations between observed and simulated
989 patterns calculated for the domain north of 20° N (to this purpose NCAR data were
990 regrided to the model grid).

991 Figure 2 – Observed and simulated correlation maps between the winter PNA index and
992 winter surface-air-temperature time series for the period 1950-2005. Dots mark grid
993 points where the correlation is not significant at 95% confidence accounting for
994 autocorrelation. The green contours mark the boxes used for the TT2010 reconstruction.
995 In panels b-i, the numbers reported in the title are the spatial correlations between
996 observed and simulated patterns calculated for the shown land-only domain north of 12°
997 N (to this purpose NCAR data were regrided to the model grid).

998 Figure 3 – Observed and simulated correlation maps between the winter PNA index and
999 winter precipitation time series for the period 1950-2005. Dots mark grid points where
1000 the correlation is not significant at 95% confidence accounting for autocorrelation. The
1001 green contours mark the boxes used for the TT2010 reconstruction. In panels b-i, the
1002 numbers reported in the title are the spatial correlations between observed and simulated
1003 patterns calculated for the shown land-only domain north of 12° N (to this purpose
1004 NCAR data were regrided to the model grid).

1005 Figure 4 – Simulated, reconstructed and pseudo-reconstructed evolutions of the winter
1006 (djf) PNA index. a) smoothed PNA time series from the simulations for the whole last
1007 millennium; b) comparison between smoothed and, then, normalized (over the period
1008 1725-1999) PNA time series from the simulations and the TT2010 reconstruction; c)
1009 comparison between normalized (over the period 1950-1999) pseudo-reconstructions
1010 (shown as agreement between pseudo-reconstructions from all the simulations) and the
1011 TT2010 reconstruction. Smoothing in panels a and b was performed through an 11-year
1012 running moving average. Dots in panel a individuate, for each simulation, occurrences of
1013 prolonged periods of positive PNA (defined as periods where the normalized smoothed
1014 index is above 1 for at least 15 consecutive years). The red bar in panels b and c
1015 highlights the approximate period of the simulations-reconstruction discrepancy.

1016 Figure 5 – Running-window (31-year) correlations of the winter (djf) PNA with winter
1017 NPI (a), NAO (b) and SOI (c) indices for simulations (colored lines) and reanalysis
1018 (black thick lines) data. Dots mark when correlation is statistically significant at 95%
1019 confidence accounting for autocorrelation.

1020 Figure 6 – Fractions of total variance of winter North American surface air temperatures
1021 (land only grid points within the domain 20-70°N, 190-300°E) explained by winter PNA,
1022 NPI, NAO and SOI indices for individual models. Values are calculated over decadal-
1023 paced 30-year periods.

1024 Figure 7 – Skill metrics (coefficient of determination (R^2_v) and coefficient of error (CE))
1025 of the ensemble PNA pseudo-reconstructions for the full-validation period. Different
1026 panels illustrate results from different reconstruction designs, summarized on the title of
1027 each panel: a) reconstructions based on geophysical predictors from northwestern North
1028 America, with R^2_c comparable to that of the actual TT2010 reconstruction (see methods);
1029 b) same as panel a, but for best R^2_c values; c) best R^2_c values from an idealized design
1030 including a temperature predictor over Florida. The numbers inside each panel indicate
1031 the minimum and maximum R^2_v values obtained for each model. Insets in each panel
1032 map the three boxes from where gridded data are sampled to be included as predictors,
1033 with the name reported in each box (tas: surface air temperature, pr: precipitation).

1034 Figure 8 – Skill metric (R^2) for an ensemble of PNA reconstructions based on
1035 geophysical predictors from northwestern North America for subsequent 30-year periods
1036 (paced at 3-decade intervals). To be comparable with TT2010, only the subset of
1037 reconstructions with R^2 for the 1950-1999 calibration period in the range [0.45-0.55] are
1038 shown, as for Figure 7a. For each 30-year period, dots are minimum, mean and maximum
1039 of R^2 values, vertical lines indicate the inter-quartile interval of R^2 values. The top
1040 symbols indicate 30-year periods when the R^2 value for NPI (square), SOI (triangle) or
1041 NAO (circle) is, for at least one predictor set, better than the worse PNA value.

1042 Figure 9 – Pseudo-reconstructions' accuracy in describing interdecadal positive PNA
1043 phases. Histograms are ensemble (all simulations) empirical probability distributions of
1044 residuals (predicted value minus true value) from the winter PNA pseudo-reconstructions
1045 obtained following an approach similar to TT2010 and illustrated in Figures 7a and 8 for
1046 (a) target 21-year smoothed PNA values above the 90th percentile and (b) pseudo-
1047 reconstructed 21-year smoothed PNA values above the 90th percentile. The black vertical
1048 lines indicate the full-period average residuals from individual simulations. 90th
1049 percentiles are calculated over the full simulation and therefore reflect also full-period
1050 biases in the pseudo-reconstructions. The smoothing is meant to mimic the approximately
1051 20-year duration of the early-19th-century positive PNA phase in the TT2010
1052 reconstruction. The considered positive PNA phases are sampled throughout the
1053 simulations, regardless of their timing.

1054 Figure 10 – Power spectral density of the winter PNA index (blue line) for individual
1055 simulations with associated 95% confidence level (blue dashed line) and agreement
1056 between the spectra of the pseudo-reconstructions (shading) obtained following an

1057 approach similar to TT2010 and illustrated in Figures 7a and 8. Agreement is defined, for
1058 a given frequency, as the fraction of total pseudo-reconstructions having power within 0.1
1059 units²/year intervals. All indices are standardized according to the 1950-1999
1060 climatology.

1061 Figure 11 – Correlation maps between the ensemble-average residuals (predicted value
1062 minus true value) from the winter (djf) PNA pseudo-reconstructions obtained following
1063 the TT2010 approach and illustrated in Figures 7a and 8 and winter surface-air-
1064 temperature time series for the pre-industrial period up to 1849. Dots mark grid points
1065 where the correlation is not significant at 95% confidence accounting for autocorrelation.
1066 The green contours mark the boxes used for the TT2010 reconstruction.